Original Article

MOLECULAR METABOLISM

Dopamine neuronal protection in the mouse *Substantia nigra* by GHSR is independent of electric activity

Bernardo Stutz [1,], Carole Nasrallah [1,2], Mariana Nigro [3], Daniel Curry [4], Zhong-Wu Liu [1], Xiao-Bing Gao [1], John D. Elsworth [4], Liat Mintz [5], Tamas L. Horvath [1,2,3,6,7,*]**

ABSTRACT

Objective: Dopamine neurons in the *Substantia nigra* (*SN*) play crucial roles in control of voluntary movement. Extensive degeneration of this neuronal population is the cause of Parkinson's disease (PD). Many factors have been linked to *SN* DA neuronal survival, including neuronal pacemaker activity (responsible for maintaining basal firing and DA tone) and mitochondrial function. DIn-101, a naturally occurring splice variant of the human ghrelin gene, targets the ghrelin receptor (GHSR) present in the *SN* DA cells. Ghrelin activation of GHSR has been shown to protect *SN* DA neurons against 1-methyl-4-phenyl-1,2,5,6 tetrahydropyridine (MPTP) treatment. We decided to compare the actions of DIn-101 with ghrelin and identify the mechanisms associated with neuronal survival.

Methods: Histologial, biochemical, and behavioral parameters were used to evaluate neuroprotection. Inflammation and redox balance of *SN* DA cells were evaluated using histologial and real-time PCR analysis. Designer Receptors Exclusively Activated by Designer Drugs (DREADD) technology was used to modulate *SN* DA neuron electrical activity and associated survival. Mitochondrial dynamics in *SN* DA cells was evaluated using electron microscopy data.

Results: Here, we report that the human isoform displays an equivalent neuroprotective factor. However, while exogenous administration of mouse ghrelin electrically activates *SN* DA neurons increasing dopamine output, as well as locomotion, the human isoform significantly suppressed dopamine output, with an associated decrease in animal motor behavior. Investigating the mechanisms by which GHSR mediates neuroprotection, we found that dopamine cell-selective control of electrical activity is neither sufficient nor necessary to promote *SN* DA neuron survival, including that associated with GHSR activation. We found that DIn101 pre-treatment diminished MPTP-induced mitochondrial aberrations in *SN* DA neurons and that the effect of DIn101 to protect dopamine cells was dependent on mitofusin 2, a protein involved in the process of mitochondrial fusion and tethering of the mitochondria to the endoplasmic reticulum.

Conclusions: Taken together, these observations unmasked a complex role of GHSR in dopamine neuronal protection independent on electric activity of these cells and revealed a crucial role for mitochondrial dynamics in some aspects of this process.

Keywords Parkinson's; Mitochondrial dynamics; Dopamine neuron; Mitofusin 2; GHSR

1. INTRODUCTION

Parkinson's Disease (PD) is a neurodegenerative disease affecting approximately 5–6 million individuals worldwide [1]. This number is expected to escalate to ~10 million by the year 2030 as the world's population rapidly ages [2]. In the United States, more than 1 million individuals have PD, and around 60,000 new cases are diagnosed every year, causing a rapidly expanding social, medical, and financial burden. Clinical features of PD include resting tremor, muscle rigidity, bradykinesia, and postural instability, usually appearing when levels of dopamine (DA) in the dorsal striatum display a 70–80% reduction [3–5], making it very difficult for PD to be detected at early stages. Parkinson's disease etiology is still elusive, and clinical interventions are focused on symptoms management rather than halt of disease progression. Appearing on the clinical scene in the late 60's, L-DOPA administration was the first proposed treatment for PD and is still largely used today, as no major development has occurred regarding effective new treatments [6]. Therefore, a better understanding of how

[1]Program in Integrative Cell Signaling and Neurobiology of Metabolism, Department of Comparative Medicine, USA [2]Interdepartmental Neuroscience Program, USA [3]Department of Obstetrics, Gynecology and Reproductive Sciences, USA [4]Department of Psychiatry, USA [5]DiaLean East Brunswick, NJ, USA [6]Department of Neuroscience, Yale University School of Medicine, New Haven, CT 06520, USA [7]Department of Anatomy and Histology, University of Veterinary Medicine, Budapest, 1078, Hungary

*Corresponding author. Brady Memorial Laboratory (BML), 330 D. 310 Cedar Street, PO BOX 208016, New Have, CT 06520, USA. Fax: +(203) 785 7499. E-mail: tamas.horvath@yale.edu (T.L. Horvath).

**Corresponding author. Brady Memorial Laboratory (BML), 330 D. 310 Cedar Street, PO BOX 208016, New Have, CT 06520, USA. Fax: +(203) 785 7499. E-mail: bernardo.stutz@yale.edu (B. Stutz).

Received December 23, 2018 • Revision received February 15, 2019 • Accepted February 16, 2019 • Available online 21 February 2019

https://doi.org/10.1016/j.molmet.2019.02.005

Abbreviations

PD	Parkinson's Disease
SN	*Substantia nigra*
MPTP	1-methyl-4-phenyl-1,2,5,6 tetrahydropyridine
GHSR	ghrelin receptor
DREADD	Designer Receptors Exclusively Activated by Designer Drugs
Drp1	dynamin-related protein 1
Mfn	mitofusin
Mff	mitochondrial fission factor
Fis-1	mitochondrial fission 1
OPA-1	Dynamin-like 120 kDa protein mitochondrial
DAP	2,3-diaminopropionic acid
TH	tyrosine hydroxylase
IBA1	ionized calcium binding adaptor molecule 1
CD 68	glycoprotein cluster of differentiation
CCL-2	C-C motif chemokine ligand 2
TNFa	Tumor necrosis factor alpha
DHE	dihydroethidium
ROS	reactive oxygen species
SOD2	superoxide dismutase 2
UCP	uncoupling protein
DAT	dopamine-associated transporter
CNO	clozapine-N-oxide
GOAT	ghrelin-O-acyl-transferase
RNS	reactive nitrogen species

substantia nigra (*SN)* DA neurons behave and respond to stimuli that may interfere with disease development will likely support the improvement of current clinical approaches.

Structurally similar to ghrelin, Dln-101 is a proprietary 24—amino acid, acylated peptide derived from a naturally occurring splice variant of the human ghrelin gene. Julst like ghrelin, Dln101, targets the growth hormone secretagogue 1 receptor (GHSR), present in hypothalamic centers controlling energy metabolism and food intake [7—9] as well as in the SN [10], a brain region where dopamine (DA) cell degeneration leads to PD. Activation of GHSR has been shown to protect *SN* DA neurons against 1-methyl-4-phenyl-1,2,5,6 tetrahydropyridine (MPTP) treatment [11—14]. The presumable mechanisms underlying GHSR-mediated neuroprotection in rodents include activation of UCP2 and associated decrease in mitochondrial ROS production [12], suppression of the pro-inflammatory cytokines TNFa, IL-6 and IL-1b [15,16], prevention of MPTP-induced increase in apoptosis-promoting factors caspase-3 and bax, as well as decrease in the anti-apoptotic gene bcl-2 [11], and augmentation of midbrain dopamine neuron electrical activity [17—19], since there is a growing body of evidence suggesting that the mechanisms that control electrical activity of *SN* DA neurons are not only crucial for regulating dopamine release in the dorsal striatum [20] but also for the survival of these neurons [21].

Finally, it is well established that mitochondria have a central role in substrate oxidation and energy production with broad consequences for whole cellular physiology [22]. The fission/fusion dynamics of mitochondria are critical not only for controlling mitochondrial shape, size, and number, but also for contributing to the dilution and sequestration of mitochondrial damage, impacting directly its function [23,24]. Fission, for example, facilitates the distribution of mitochondria in response to local demand for ATP, whereas fusion helps to replace damaged mtDNA and to regenerate damaged/depolarized mitochondria [25,26]. The fission/fusion dynamics are controlled by opposing actions of different dynamin-family members, dynamin-related protein 1 (Drp1) and mitofusins (Mfns), assisted by mitochondrial outer membrane receptors such as mitochondrial fission 1 (Fis-1) and mitochondrial fission factor (Mff) [27,28]. Dysfunctional mitochondrial fission/fusion dynamics are believed to be central to the pathophysiology of both familial and sporadic PD [29,30]. These conclusions are supported by the observation of mitochondrial dysfunction and fragmentation in postmortem studies, including altered expression of proteins related to mitochondrial dynamics [31,32], identification in PD patients of mutations in genes encoding proteins important for mitochondrial dynamics [33,34], and increased accumulation of mutations in the mitochondrial DNA of *SN* DA neurons with age and PD [35,36].

Exposure of human and animals to MPTP can reproduce all the characteristic motor and non-motor signs of PD, in addition to mimicking the same responses and side effects to drugs used to treat PD [37,38]. Anatomically, intoxication with MPTP induces the same selective loss of substantia nigra DA neurons that occurs in PD. In addition, some of the key biochemical changes elicited by MPTP treatment are the same as those identified in idiopathic and genetic forms of PD, such as deficiency in mitochondrial Complex I activity and induction of oxidative stress in DA neurons [39]. The rodent and nonhuman primate MPTP models have been used to develop both symptomatic and neuroprotective treatments for PD.

The aim of this study was to evaluate Dln101 as a potential neuroprotective compound, in comparison with ghrelin, and investigate its GHSR-mediated effects that increase *SN* DA resilience to MPTP. Although Dln101-mediated neuroprotection of *SN* DA cells was equivalent to that of ghrelin, its effect on electrical activity, dopamine release, locomotor behavior, and modulation of mitochondrial dynamics were very distinct despite the requirement of GHSR in mediating both molecules effects.

2. MATERIALS AND METHODS

2.1. Materials

Otherwise stated, all chemical were purchased from Sigma Aldrich (St. Louis. MO, USA). Dln101 and ghrelin were obtained from Peptides International (Louisville, KY, USA). CNO was obtained from Enzo Life Sciences and Salvinorin B from Cayman chemicals.

2.2. Animals

All animal procedures were performed in accordance to the National Institutes of Health Guide for the Care and Use of Laboratory Animals in research and were approved by the Institutional Animal Care and Use Committee of Yale University. All mice were handled once a day for three days prior to the start of experimental procedures for acclimation purposes. Mice harboring the dopamine-associated transporter-cre recombinase transgene (DAT-cre), the tamoxifen-inducible dopamine-associated transporter-cre (iCre-DAT), and the ribotag allele ribotag were all obtained from Jax mice. DAT-cre-ribotag and iCre-DAT-ribotag animals permit, in a cre-dependent fashion (expressed in dopamine neurons), the immunoprecipitation of ribosome-associated mRNA. Mitofusin 2 (mfn2) floxed animals were available in our lab, as previously described [40]. Whole-body GHSR KO mice were also available in our laboratory [41].

2.3. Genotyping

DNA was obtained from toe biopsy. Genomic DNA (gDNA) was extracted and standard PCR was performed using REDExtract-N-Amp™ Kit (Sigma). Cre recombinase, HA-RPL22, and Mfn2 gene presences were assessed according to PCR protocol from Jackson Laboratories. For Cre recombinase transgene, primers did not distinguish heterozygous from homozygous animals. Cre primers used were oIMR1084 (5′-GCGGTCTGGCAGTAAAAACTATC-3′) and oIMR1085 (5′-GTGAAACAGCATTGCTGTCACTT-3′). For HA-RPL22, primers used were 9508 (5′-GGGAGGCTTGCTGGATATG-3′) and 9509 (5′-TTTCCAGACA-CAGGCTAAGTACAC-3′). For Mfn2, primers were HC106 (5′-GAAG-TAGGCAGTCTCCATCG-3′) and HC 107 (5′-AACATCGCTCAGCCTG-AACC-3′). For mCAT, primers were 18290 (5′-CGGTGTGGA-CAACCACTACA-3′) and 18291 (5′-TCAGGAATTCTCTCTCGGTCA-3′).

2.4. Dln101, ghrelin, and MPTP treatment

Unless otherwise indicated in text, animals were injected with ghrelin or Dln101 for a total of 10 consecutive days, subcutaneous (s.c.), 15 min before the onset of the dark cycle, with either saline (vehicle), ghrelin (15nmoles), or Dln101 (15nmoles) and had their food removed during the dark cycle. *Ad libitum* access to food was re-established in the next morning (8:30-9am). On the seventh day, animals were challenged with MPTP (60 mg/kg, divided in 4 doses, 3—4 h apart). Samples were processed on the morning of day 11.

2.5. Home cage monitoring

Mice were left to acclimate in TSE LabMaster home cages for at least 3 days before recording food intake, water intake, and locomotor activity.

2.6. Food intake and body weight measurement

All mice were individually caged 5 days before the start of feeding studies to allow the animals to acclimate to their new environment. Animals and food pellets were weighed daily.

2.7. Pharmacokinetic analysis

Pharmacokinetic parameters were determined by non-compartmental analysis using the software package, PK Solutions 2.0 (Summit Research Services). Area under the curve (AUC) values were calculated by the trapezoidal method. Maximal drug concentration in tissue (C_{MAX}), time to reach maximal tissue levels (T_{MAX}), apparent elimination half-life (2—6 h—sc; 2—4 h—ip), AUC and brain/plasma ratios based on AUC (0—6 h) were evaluated for plasma and brain samples at six different time points following intraperitoneal and subcutaneous administration of ghrelin or Dln101.

2.8. Immunostaining

Mice were perfused transcardially with ice-cold 0.9% NaCl saline followed by 4% paraformaldehyde, 15% picric acid (vol/vol) in 0.1M phosphate buffer (PB). Brains were removed and fixed in 4% paraformaldehyde for at least 24 h before being cut with the vibratome. Brains 50-μm-thick coronal sections were cut. Before antibody incubation, all sections were blocked in 5% normal goat serum containing 1% BSA, 0.1% glycine and 0.1% L-lysine to avoid nonspecific antibody binding, then incubated with mouse monoclonal anti-TH (1:3500, Millipore MAb 318) or rabbit polyclonal anti-IBA-1 (1:3000, Wako 019—19741). After overnight incubation at 4 °C, the sections were incubated in respective biotinylated secondary antibodies, and Vectastain ABC kit (Vector Laboratories) or Avidin conjugated to Alexa 488. For visualization after ABC kit, DAB and glucose oxidase were used. All staining was visualized by Axio Scope 1 (Zeiss) and analyzed using ImageJ.

2.9. *In situ* detection of reactive oxygen species

Dihydroethidium (Molecular Probes, Eugene, OR) was used to investigate the local *in situ* production of reactive oxygen species (ROS), because it is specifically oxidized by superoxide to red fluorescent ethidium. An intravenous injection of 200 μl of dihydroedithium (DHE; stock solution, 1 mg/ml in 1% DMSO vehicle) was administered through the tail vein to lightly restrained mice. Three hours after DHE injection, mice were perfused and processed for immunostaining, as described.

2.10. Stereological analysis

The *SN* was delineated from −2.54 to −3.88 mm from Bregma according to Paxinos Atlas for the mouse brain [42]. The number of TH^+ cells in *SN* was estimated counting every other section throughout the rostro-caudal extent of the *SN*.

2.11. Electron microscopy

Under deep anesthesia, mice were perfused transcardially with ice-cold 0.9% NaCl saline followed by 4% paraformaldehyde, 15% picric acid (vol/vol), and 0.1% glutaraldehyde (vol/vol) in 0.1M PB, and processed and labeled for immunostaining, except for the addition of a freeze-thaw step to disrupt cellular membranes before the incubation with the primary antibody. Sections were subsequently osmicated and dehydrated, and ultrathin sections were cut on a Leica Ultra-Microtome, collected on Formvar-coated single-slot grids and analyzed with a Tecnai 12 Biotwin transmission electron microscope (TEM - FEI).

2.12. Morphological analysis of mitochondria within *SN*

Measurements were generated from five to ten randomly acquired TEM images. The morphology of each mitochondrion was analyzed using ImageJ software. Mitochondria were identified by presence of identifiable cristae and distinct double membrane; mitochondria with unclear morphology were excluded from the analysis.

Mitochondrial morphology parameters and terms: "mitochondrial area" = area of every individual mitochondria. "Average mitochondrial area" = summation of the area of every mitochondria divided by the total number of mitochondria, i.e. arithmetic mean."Cytoplasm area" = cell area − nucleus area. "Mitochondrial cytoplasmic coverage" = summation of the area of every mitochondria divided by the cytoplasm area, in percentage. Two types of analysis were made: using histogram curves to describe and compare the distribution of the mitochondria population between groups and comparing the averages between groups.

2.13. Rotarod

The AccuRotor Rota Rod (Accuscan Instruments, Columbus, OH) apparatus consists of a rotating bar located 20 cm above the floor. On days 1—6, all mice were trained on the rotarod (three trials per day, initial speed = 0 rpm, maximum speed = 25 rpm, time to reach maximum speed = 90 s). The cut-off time on the rotarod was 180 s. The latency to fall from the rotating bar was recorded. The average latency of both last two trials in each day was used for analyzes.

2.14. High performance liquid chromatography (HPLC) determination of neurotransmitters dopamine, serotonin, and their metabolites

Mice were euthanized, and brain tissue was dissected and snap-frozen using liquid nitrogen. Samples were sonicated in 200 μL of 0.1N perchloric acid and 0.1 ng of 3,4-dihydroxybenzylamine hydrobromide (DHBA, as internal standard); after centrifugation at 14,000 xG for

15 min, the supernatant was filtered through 0.22 μm syringe filter (PALL Corp. PN4454). Tissue level of neurotransmitters was measured by HPLC analysis coupled with electrochemical detection as described [43]. Fast isocratic separation was obtained using a reverse phase Agilent HC-C18 column (5 μm particle size; Agilent Technologies) with the following mobile phase: 30 mM sodium citrate, 13.7 mM sodium monobasic phosphate, 0.025 mM Na_2EDTA, 0.75 mM sodium octanesulphonate; pH 3.15–3.2, containing 0.6% tetrahydrofuran, 0.1% diethylamine and 6.5% acetonitrile.

2.15. Acute brain slice preparation and electrophysiology

Coronal brain slices (250 μm) were prepared from 4- to 8-week-old animals for all genotypes tested. The slices were sectioned into ice-cold oxygenated (5% CO_2, 95% O_2) dissection buffer (in mM: 87 NaCl, 2.5 KCl, 1.6 NaH_2PO_4, 25 $NaHCO_3$, 75 sucrose, 10 glucose, 1.3 ascorbic acid, 0.5 $CaCl_2$, 7 $MgCl_2$), recovered for 15 min at 37 °C in oxygenated artificial cerebrospinal fluid (aCSF) (in mM: 122 NaCl, 3 KCl, 1.2 NaH_2PO_4, 26 $NaHCO_3$, 20 glucose, 2 $CaCl_2$, 1 $MgCl_2$, 305–310 mOsm, pH 7.3) and acclimated at room temperature for 10 min before performing electrophysiological recordings. Borosilicate glass electrodes (Sutter Instruments, Novato, CA) were used for whole cell patch clamp recordings. Electrodes were pulled with tip resistance of 2 MΩ, and filled with internal solution (in mM, 120 K-gluconate, 5 KCl, 2 $MgCl_2$, 0.05 EGTA, 10 HEPES, 2 Mg-ATP, 0.4 Mg-GTP, 10 creatine phosphate, 290–300 mOsm, pH 7.3). During recordings, coronal brain slices were placed in a room temperature chamber mounted on an Olympus upright microscope (BX50WI) and perfused with oxygenated aCSF. Cells were visualized under differential interference contrast imaging. Data were obtained via a Multiclamp 700B amplifier, low-pass Bessel-filtered at 4 kHz, and digitized on computer disk (Clampex, Axon Instruments).

2.16. Real-time PCR

Gene expression was investigated using real-time qPCR, performed in 96 or 384-well PCR plates using the Roche 480 LightCycler Thermal Cycler. The real-time PCR reaction mixture contained iTaq SYBR green master mix (BioRad), 0.3 mM primer pairs, and diluted cDNA in a total volume of 10 μl. The mixture was heated initially to 95 °C for 3 min to activate hot-start iTaq DNA polymerase and then followed by 50 cycles with denaturation at 95 °C for 10 s, annealing and extension at 60 °C for 60 s. Samples and standards were run in triplicate. Primers were carefully designed to span exon-exon junction in the mRNA and intron-spanning in the gDNA, when possible. Briefly, NCBI Primer-Blast was used, and gene and mRNA sequences were obtained from NCBI website. Primers were tested for efficiency, specificity, and primer dimer formation using 10-fold dilution curve of cDNA concentration. Additionally, a melt curve protocol designed for increment temperatures of 0.5 °C with a starting temperature of 57 °C and ending at 92 °C was performed at the end of all PCR-reactions. RNA was extracted from target tissues using RNeasy Micro Kit (QIAGEN #74004) and cDNA was synthesized using Quantitect Reverse Transcription kit (QIAGEN #205311). Real-time PCR analysis was made using the comparative threshold cycle method (ΔΔCt) with actin as reference gene. Potential reference genes, including actin, cyclophilin A, beta-2 microglobulin, glyceraldehyde-3-phosphate dehydrogenase (gapdh), and riosomal 18S were tested and actin was found to show the least variation among samples. Selected human RNA samples (Kidney, Pancreas, Stomach, Duodenum, Placenta, and non commercial A172 glioblastoma cell line - Brain) were obtained from Stratagene. Primer sets were: Actin F(+)AGTGTGACGTTGACATCCGTA, R(−)GCCAGAGCAGTAATCTCCTTCT; IL1α F(+)CGCTTGAGTCGGCAAAGAAA, R(−)ACTCCCGAAATAAGGCTGCT; IL1β F(+) AAGAGCTTCAGGCAGGCAGTATCA, R(−)ATGAGTCACAGAGGATGGGCTCTT; TNFa F(+)AGACCCTCACACTCAGATCA, R(−)TGTCTTTGAGATCCATGCCG; IFNγ F(+) CCTAGCTCTGAGACAATGAACG, R(−)TTCCACATCTATGCCACTTGAG; IL6 F(+)AGACAAAGCCAGAGTCCTTCAGAG, R(−)TTGGTCCTTAGCCACTCCTTCTGT; IL18 F(+)CGACTTCACTGTACAACCGCAGTA, R(−) CACAGCCAGTCCTCTTACTTCACT; Nlrp3 F(+)ATGCTGCTTCGACATCTCCT, R(−)AACCAATGCGAGATCCTGAC; CD68 F(+)GTGTCTGATCTTGCTAGGACC, R(−)TGTGCTTTCTGTGGCTGTAG; Ccl2 F(+)GGAGAGCTACAAGAGGATCAC, R(−)TGATCTCATTTGGTTCCGATCC; Ccl5 F(+) AGATCTCTGCAGCTGCCCTCA, R(−)GGAGCACTTGCTGCTGGTGTAG; SOD2 F(+)CAATAATGTTGTGTCGGGCG, R(−)CATGATCTGCGCGTTAATGTG; Catalase F(+)CCCTCGGACTTTGGCAAA, R(−)CCAGACTCGAGTATCGCTGACA; Gluthathione Peroxidase F(+)GGAAGCCACATTCCCAGTCA, R(−)GTGCCAAGCCGTAAACACAG; PGC1α F(+)CCCTGCCATTGTTAAGACC, R(−)TGCTGCTGTTCCTGTTTTC; ucp2 F(+) GCATTGGCCTCTACGACTC, R(−)AAGCGGACCTTTACCACATC; ucp3 F(+)GTTCCTTTGCTGCCTATGGA, R(−)TACCCAACCTTGGCTAGACG; ucp4 F(+) CCGCCATTTACAGACACGTAG, R(−)TCCAATGACCGATTTCCAGAG; ucp5 F(+)GAAACCTTTTGTGTATGGCGG, R(−)AACATCGATACTCTGGCCTTG; Fis-1 F(+)AGCTGGTTCTGTGTCCAAG, R(−)TGTTCCTCTTTGCTCCCTTTG; MFF F(+)CTAATCTTTCCTCTGCCCGTG, R(−)GATGAGGATTAGAAGTGGCGG; Drp-1 F(+)TCCCAATTCCATTATCCTCGC, R(−)CATCAGTACCCGCATCCATG; Mfn1 F(+)GGATAATGCAGCCCAGGAG, R(−) GACAGAGATTAGTTTCCAGCCC; Mfn2 F(+)CATCCCCAGTTGTCCTCAAG, R(−)TTCAAGCCGTCTATCATGTCC; OPA-1 F(+)GTGTGCTGGAAATGATTGCTC, R(−)TGGTGAGATCAAATTCCCGAG;

2.17. Viral vectors and stereotaxic injections

DAT-cre-ribotag mice were anesthetized with a ketamine/xylazine cocktail and injected into the *SN* (coordinates from Bregma − AP: 3.6; ML: ±1.4; DV: 4.0 and AP: 3.65; ML: ±1.2; DV: 4.2) with 500 nL of excitatory DREADD virus (rAAV5-hSyn-DIO-hM3Dq-mCherry; 5×10^{12} vg/ml), 500 nL of inhibitory DREADD virus (rAAV9-hSyn-DIO-KORD-IRES-mCitrine; 5.3×10^{12} vg/ml), or the control virus lacking the DREADD construct rAAV5-hSyn-DIO-mcherry (5×10^{12} vg/ml) (UNC Vector Core, Chapel Hill, NC). DREADD receptors are only expressed in cre recombinase-positive cells, and due to spatial localization of the viral injection, this procedure allows the expression of DREADDs exclusively in *SN* DA neurons. Mice were allowed to recover for approximately ten days and then injected daily subcutaneously 15 min before the onset of the dark phase, with either clozapine-N-oxide (CNO, excitatory DREADD agonist 0.3 mg/kg, ENZO Life Sciences) or 0.9% saline vehicle control; or Salvinorin B (inhibitory DREADD agonist 5 mg/kg, Cayman Chemical) or DMSO vehicle control, for seven consecutive days, permitting chemicogenetic excitation of *SN* DA cells with CNO or inhibition of *SN* DA cells with salvinorin B. In addition, for chronic and continuous release of either CNO or Salvinorin B, mice were implanted with subcutaneous osmotic mini-pumps (Alzet). Viral vector placement was assessed via florescent microscopy based on mouse brain atlas landmarks.

2.18. Osmotic mini pump implantation

Before implantation, the Alzet osmotic minipumps (Model 1007D; pumping rate, 0.5 μL/h for seven days) were filled with the appropriate solution and incubated at 37 °C for 24 h for priming and flow stabilization. At the time of the surgery, mice were given intraperitoneal injection of ketamine/xylazine (0.3 mL), and had the pump subcutaneously implanted in the space between the scapulae.

2.19. Statistics

Data are expressed as mean ± SEM unless otherwise indicated. GraphPad Prism 7 was used for all statistical analysis, and we considered $p < 0.05$ as statistically significant; labeled as: * = $p < 0.05$, ** = $p < 0.01$, *** = $p < 0.001$. When ANOVA was performed, post-hoc test was used to compare the mean of each column to the mean of the control column and correcting for multiple comparisons using the Tukey test. When comparing the mean of each column to the mean of every other column, letters (*a,b,c*) were used to indicate differences; unless otherwise indicated in the figure legend.

3. RESULTS

3.1. Dln101 is a human splice-variant of the ghrelin gene with different expression pattern but similar effects over food intake and body weight gain

Structurally similar to ghrelin, Dln101 is an acylated 24-amino acid peptide that is derived from a naturally occurring splice variant of human ghrelin. To increase the stability of Dln101 peptide, the ester bond between the serine at position 3 (Ser3) and the n-octanoyl group was modified to an amide bond, resulting in replacement of Ser3 by 2, 3-diaminopropionic acid (DAP) (Figure 1A). Dln101 mRNA expression pattern also differs from the one observed for ghrelin. Ghrelin is mainly expressed in gastro-intestinal (GI) organs and, to a lower extent, in kidney and neural tissue. Dln101 had low to no expression in the GI tract but displayed elevated expression in kidney and neural tissue (Figure 1C). When administered to mice for 7 consecutive days, Dln101 displayed an effect similar to ghrelin, promoting increases in body-weight. We also observed a positive trend (at day 6, $p = 0.09$; at day 7 $p = 0.056$) in cumulative food intake (Figure 1B).

Next, we decided to compare acylated Dln101 (henceforth Dln101) and acylated ghrelin (henceforth ghrelin) plasma pharmacokinetic concentrations, following subcutaneous and intraperitoneal administrations as shown in Table 1. Absorption was rapid across all doses with T_{MAX} at 5 min. Intraperitoneal (i.p.) injections of 1.2 and 7.2 mg/kg of Dln101 raised plasma concentration to peak (C_{MAX}) at 36.3 and 588 ng/ml. Ghrelin i.p. injections reached C_{MAX} at 7.5 and 171.4 for 1.2 and 7.2 mg/kg doses, respectively. Subcutaneous (s.c.) injections of Dln101 displayed similar PK parameters when compared to i.p. injections. Increases in both AUC and C_{MAX} were proportional to administered dose and route, with s.c. administrations displaying higher C_{MAX} and AUC for 7.2 mg/kg dosage. Mean half-life of Dln101 ranged between 11.9 and 20.9 min compared to 14.8 for ghrelin.

3.2. Dln101 protects *SN* DA neurons against MPTP-induced degeneration, inflammation, and increased ROS production

Initially, we evaluated neuroprotection of *SN* DA neurons by ghrelin and Dln101 by counting *SN* tyrosine hydroxylase-positive (TH^+) neurons in brain sections from mice injected, s.c., for 10 consecutive days, 15 min before the onset of the dark cycle, with either saline (first and second bar on the graph), ghrelin (15nmoles), or Dln101 (15nmoles). On day 7, animals were challenged with MPTP (60 mg/kg, i.p.), or not (control group). MPTP injection promoted vast nigral degeneration in vehicle-treated animals, with 55.9% reduction in TH^+ cells, equally mitigated by either ghrelin or Dln101 pre-treatment, with 19.8% and 16% reduction, respectively (Figure 2A,B). Preservation of motor

Table 1 — Pharmacokinetic profile of Dln101 and ghrelin. T_{MAX} = time of maximal plasma concentration, C_{MAX} = maximal plasma concentration, $AUC_{0-\infty}$ = area under the plasma concentration *vs* time curve from time 0 to infinity, $T_{1/2}$ = half-life.

PEPTIDE	DOSE (mg/Kg)	ROUTE	T_{MAX} (min)	C_{MAX} (ng/mL)	$AUC_{0-\infty}$ (ng.min/mL)	$T_{1/2}$ (min)
Dln101	1.2	*i.p.*	5	36.3	622	20.9
	7.2			588	9160	11.9
	7.2	*s.c.*		828	16106	12.6
Ghrelin	1.2	*i.p.*		7.5	NA	NA
	7.2			171.4	40788	14.8

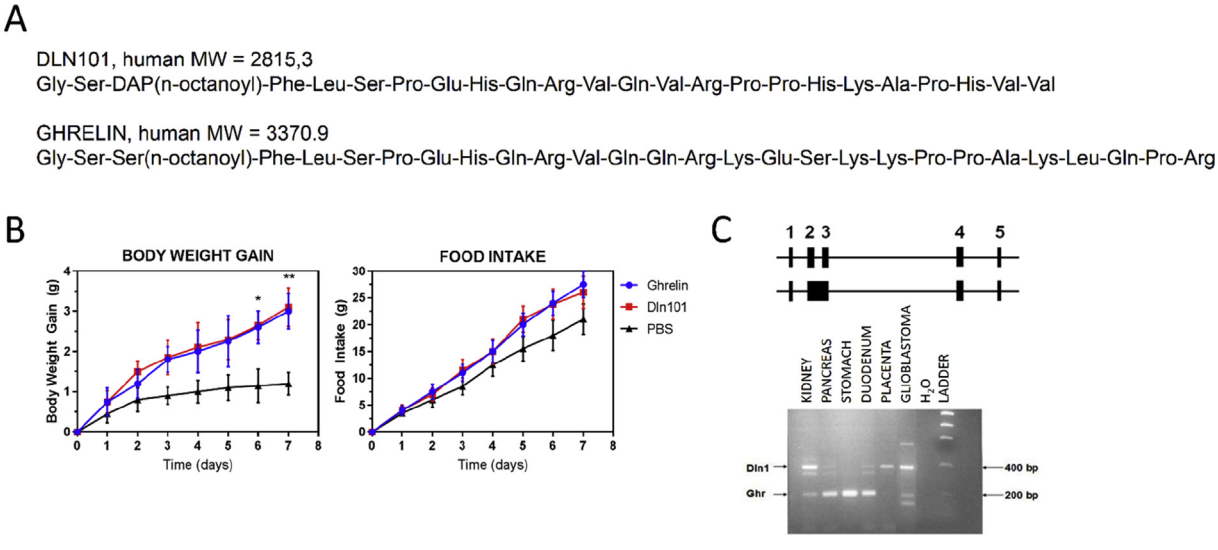

Figure 1: Dln101 is a human splice-variant of the ghrelin gene with different expression pattern but similar effects over food intake and body weight gain. (A) Dln101 and ghrelin peptide sequences. Mature peptides display homology of 57% and same acylation site in the third residue. **(B)** Chronic peripheral (s.c.) injection of Dln101 or ghrelin (7.2 mg/kg) had similar effects on Body Weight Gain and Food Intake in mice. Two-way ANOVA followed by multiple comparisons test; n = 8 per group. **(C)** Human ghrelin gene mRNA splicing and their respective expression pattern. Two splicing patterns of ghrelin mRNA. The boxes represent exons, short boxes represent untranslated sequences, and long boxes represent coding sequences. Top pattern yields mature ghrelin 117 amino acids preproghrelin, while bottom pattern yields Dln. Qualitative RT-PCR was conducted on 6 selected human samples (Stratagene: Kidney, Pancreas, Stomach, Duodenum, Placenta, and non-commercial A172 glioblastoma cell line — neural tissue). Water was used as negative control. Dln and ghrelin bands are indicated with arrows.

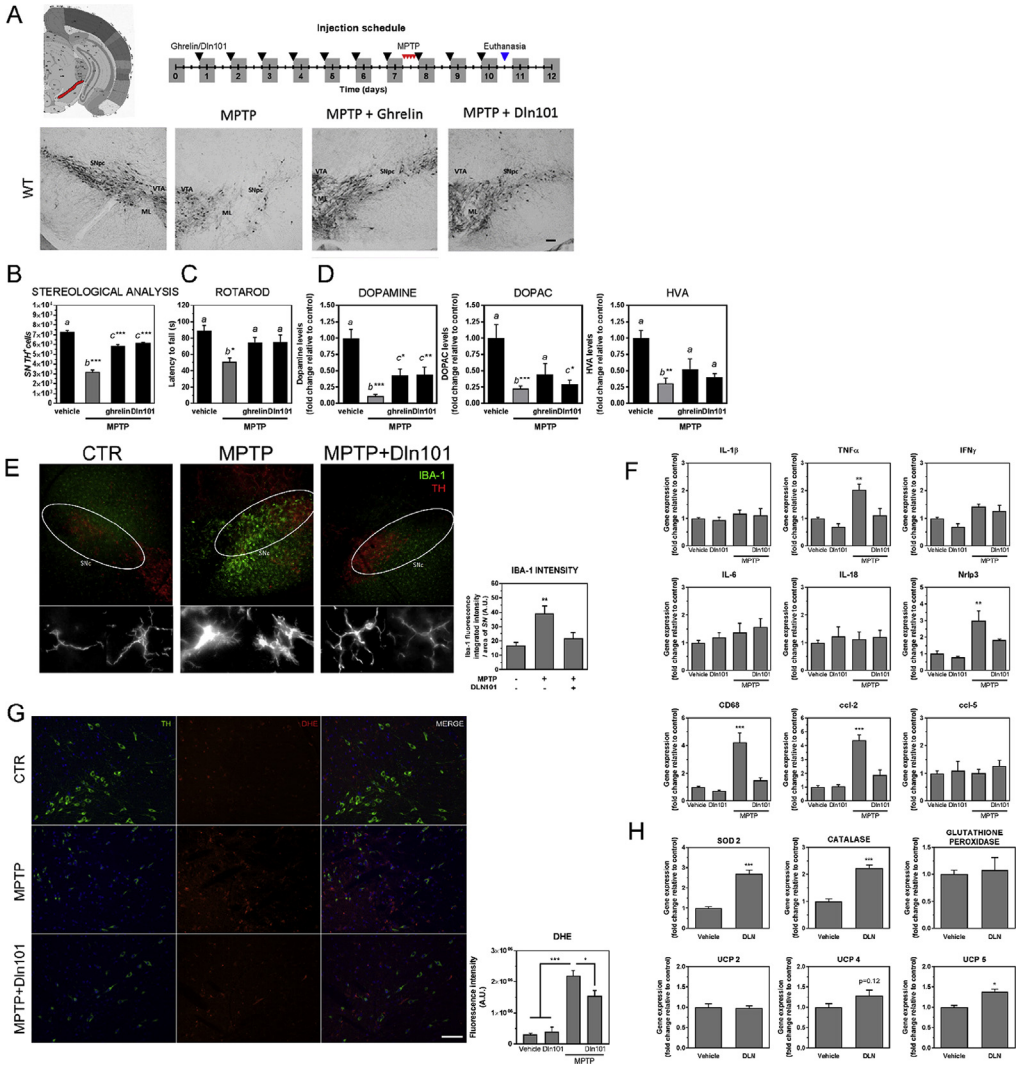

Figure 2: Neuroprotective effect of ghrelin and Dln101 in WT mice. Mice had daily s.c. administration of saline, ghrelin 15 nM, or Dln101 15 nM 15 min before the onset of dark phase for 10 consecutive days. **(A)** Visualization of TH^+ cells in DAB immunohistological preparation. Scale bar 100 μm. Parameters from DA cells of the *SN* but not from VTA were analyzed. The distinction was made visually, as indicated. SNc (*Substantia nigra pars compacta*), VTA (Ventral Tegmental Area), ML (Medial Lemniscus). **(B)** Total number of TH^+ cells in *SN* was evaluated. MPTP-treated animals, pre-treated with saline (gray bars), displayed a reduction in the number of *SN* DA cells when compared to controls (vehicle = 7305 ± 128; MPTP = 3222 ± 200). Animals pre-treated with either ghrelin or Dln101 displayed comparable levels of *SN* DA cell protection (ghrelin = 5857 ± 129, Dln101 = 6139 ± 84, TH^+ cells); n = 5–10 per group. **(C)** Motor performance was evaluated using the rotarod test. Latency to fall from the apparatus was measured in all groups. MPTP-treated animals, pre-treated with saline (gray bars), displayed a reduction in latency to fall time when compared to controls (vehicle = 88.9 ± 6.4; MPTP = 51.0 ± 5.0, in seconds). Animals pre-treated with either ghrelin or Dln101 displayed comparable levels of motor performance, with a lower reduction in latency to fall time (ghrelin = 74.4 ± 6.4, Dln101 = 74.7 ± 9.2, in seconds); n = 5–11 per group. **(D)** Dopamine, DOPAC and HVA levels were evaluated in dorsal striatum by HPLC-ED; n = 5–11 per group. **(E)** Microglia immunostaining using IBA-1 antibody (green) and *SN* DA cells (TH, red) scale bar 100 μm. Inset showed in higher magnification. Scale bar 10 μm. **(F)** Real-time PCR analysis of proinflammatory markers in midbrain tissue; n = 4 per group. **(G)** DHE staining of ROS in midbrain sections. Cells co-labelled with TH (green) and the ROS probe DHE (red) were analyzed for fluorescence intensity (quantification in the graph). Scale bar 50 μm. N = 4–6 per group **(H)** Real-time PCR analysis of antioxidative enzymes using DAT-Ribotag immunoprecipitated midbrain mRNA. Unpaired t test n = 4 per group. All other data were analyzed using One-way ANOVA test followed by multiple comparisons test.

behavior was evaluated using the accelerating Rotarod test, with vehicle-treated animals used as controls. A shorter latency to fall from the apparatus is indicative of motor impairment, a hallmark of MPTP-treated animals, which displayed a reduction of 42.7% in latency to fall time when compared to controls. Animals that received either ghrelin or Dln101 before MPTP challenge, displayed comparable levels of motor performance, with 16.3 and 16% reduction in latency to fall time respectively, supporting their role as being neuroprotective of the nigrostriatal dopamine system (Figure 2C). In line with these observations, dopamine levels in dorsal striatum of animals exposed to MPTP displayed a 90% reduction (Figure 2D). Animals pre-treated with ghrelin or Dln101 showed significantly attenuated dopamine depletion of 60% and 56%, respectively. Moreover, analysis of dopamine turnover products DOPAC and HVA suggests protection of dopamine release in animals pre-treated with ghrelin and Dln101 exposed to MPTP (Figure 2D).

Next, we decided to analyze Dln101 effects over *SN* DA neurons that bring about protection. Based on current literature of PD, we hypothesized that mitigation of MPTP-induced nigral degeneration by Dln101 could be achieved by dampening inflammation, regulating ROS production/detoxification, augmenting midbrain dopamine neuron electrical activity, changes in mitochondria, or any combination of

aforementioned effects. Following MPTP exposure, we observed microglial activation using ionized calcium binding adaptor molecule 1 (IBA1) immunostaining (Figure 2E) and increased levels of gene expression of activation markers, such as the glycoprotein cluster of differentiation (CD) 68 gene, the C-C motif chemokine ligand 2 (CCL-2) gene, and the inflammasome protein Nrlp3 gene. Pro-inflammatory cytokine TNFα gene also displayed increased levels after MPTP exposure. Interestingly, animals pre-treated with Dln101 displayed microglial morphology similar to vehicle-treated animals (Figure 2E) and no increase in levels of TNFα, CD68, and CCL-2 genes was observed (Figure 2F). As microglia cells are activated during cellular damage, these results suggest less microglial activation in the *SN* and, therefore, decreased overall dopaminergic cell loss in animals pre-treated with Dln101.

Accumulating evidence indicates that oxidative damage contributes to the cascade of events leading to degeneration of *SN* DA neurons. Evaluation of ROS levels using dihydroethidium (DHE) demonstrated a 7.46 fold increase in ROS (red) production in *SN* DA neurons (TH^+-green) following MPTP exposure (Figure 2G). Animals pre-treated with Dln101 displayed reduced levels of ROS (5.25 fold increase). In further investigating mRNA levels of enzymes involved in ROS production and detoxification in *SN* DA neurons using the DAT-ribotag animals, we found upregulation of superoxide dismutase 2 (SOD2) and catalase (Figure 2H), involved in detoxification of superoxide and peroxide species, respectively. No changes were observed in mRNA levels for glutathione peroxidase. Surprisingly, opposite to what has been described for ghrelin treatment, we found no changes in UCP2 mRNA levels following Dln101 treatment, an increase in mRNA levels of UCP5, and a tendency towards increase in UCP4 (Figure 2H), both also involved in uncoupling mechanisms in neuronal mitochondria and potential reduction of ROS formation.

3.3. Dln101 and ghrelin have opposite electrophysiological effects over *SN* DA neurons

During the course of characterizing GHSR-mediated effects on *SN* DA neuron physiology, we discovered that the GHSR agonist, ghrelin, and Dln101 had opposite effects on neuronal firing, while both signals act on GHSR receptors. In electrophysiological recordings, ghrelin induced an increase in the firing frequency of *SN* DA neurons, while Dln101 decreased it (Figure 3A). Neither molecule had an effect on firing activity in *SN* DA cells of GHSR KO animals (Figure 3B), suggesting the requirement of GHSR for the effect on modulation of neuronal electrical activity. To further investigate whether those effects on electrical activity of *SN* DA neurons in slice preparations for patch clamp analysis would indeed reflect in changes *in vivo* of dopamine release into the dorsal striatum and/or changes in the animals' locomotor behavior, we evaluated the effect of ghrelin and Dln101 on dopamine release in the dorsal striatum, the synaptic target of *SN* DA neurons. In line with the electrophysiology experiments, 30–45 min after subcutaneous injection, ghrelin induced an increase in dopamine release (Figure 3C-top) whereas Dln101 induced a decrease when compared to littermates injected with 0.9% NaCl (saline – CTR) (Figure 3C-bottom). Again, no change was observed in the dorsal striatum of GHSR KO mice (Figure 3D). To show specificity of modulation of the dopaminergic system, serotonin release in the dorsal striatum of WT animals was measured under the same conditions and neither ghrelin nor Dln101 induced a change (Figure 3E).

The nigrostratal dopaminergic pathway modulates both the direct and indirect pathways of motor control by basal ganglia, and dopamine release in the dorsal striatum leads to increased motor activity. To fully characterize the role of ghrelin and Dln101 in the activation of the nigrostriatal pathway and their effect over locomotor activity, WT mice were monitored using infrared monitors after ghrelin (15 nmoles) or Dln101 (15 nmoles) injection 15 min before the onset of the dark phase. As expected for scenarios of increased electrical activity of *SN* DA neurons and increased dopamine release in the dorsal striatum, animals injected with ghrelin displayed a trend towards increased locomotor activity in comparison to saline-injected mice. The opposite was found in Dln101-injected animals (Figure 3F).

3.4. Modulation of *SN* DA cell electrical activity does not interfere with MPTP-induced degeneration

The presence of GHSR was protective of *SN* dopamine neurons in the MPTP model regardless of whether the ligand electrically activated (ghrelin) or inhibited (Dln101) the dopamine neurons. We sought to verify whether dopamine neuronal activation or inactivation *per se* would impact *SN* DA neuronal survival upon MPTP-induced cellular stress. To address that, we used mice harboring the dopamine-associated transporter-cre recombinase transgene (DAT-cre), which permits control over neuronal electrical activity, in a cre-dependent fashion (expressed in dopamine neurons). DAT-cre mice were injected bilaterally into the *SN* with excitatory DREADD virus (rAAV5-hSyn-DIO-hM3Dq-mCherry; DAT-SN^{hM3q}) or inhibitory DREADD virus (rAAV9-hSyn-DIO-KORD-IRES-mCitrine; DAT-SN^{KORD}) (UNC Vector Core). DREADD receptors are only expressed in cre recombinase-positive cells, and, due to spatial localization of the viral injection, this procedure allows the expression of DREADDs exclusively in *SN* DA neurons (Figure 4A). Mice were then injected subcutaneously with either clozapine-N-oxide (CNO, excitatory DREADD agonist) or 0.9% saline vehicle control; or salvinorin B (inhibitory DREADD agonist) or DMSO vehicle control, permitting chemicogenetic excitation or inhibition of *SN* DA cells with CNO or salvinorin B, respectively. To confirm proper control of activity of *SN* DA neuronal population, we evaluated dopamine release in the dorsal striatum and locomotor activity of DAT-SN^{hM3q} (Figure 4B-top) and DAT-SN^{KORD} (Figure 4B-bottom).

To check neuroprotection of *SN* DA cells after MPTP (60 mg/kg) insult, DAT-SN^{hM3q} animals were administered subcutaneously daily for 7 consecutive days, 15 min before the onset of the dark cycle, with either vehicle (first and third bar), CNO (second and fourth bar), or had an osmotic minipump filled with CNO solution implanted (fifth bar) and then challenged with MPTP (Figure 4C). After MPTP, animals were maintained in injection protocol for additional 3 days (10 days total). Similarly, DAT-SN^{KORD} animals received either vehicle (first and third bars), Salvinorin B (second and fourth bars), or had an osmotic minipump filled with Salvinorin B solution implanted (fifth bar) (Figure 4D). The exact same procedure was performed in GHSR-KO animals injected with DREADD virus (Figure 4E,F). Control animals underwent the same injection routine but did not receive MPTP at the end of the 7 consecutive days. Quantification of *SN* DA cells (TH^+ cells) showed that neither increase nor decrease of *SN* DA cell electrical activity had any neuroprotective effect and both WT and GHSR-KO animals displayed the exact same level of MPTP-induced degeneration as observed in control animals. Additionally, we decided to use the DREADD approach to neutralize the effect of ghrelin and Dln101 over the electrical activity of *SN* DA cells and verify the impact on the neuroprotection observed with these two molecules (Figure 4A). DAT-SN^{KORD} animals treated with ghrelin and DAT-SN^{hM3q} animals treated with Dln101 had their electrical activity effect neutralized with Salvinorin B or CNO, respectively. Analysis of dopamine release in the dorsal striatum confirmed neutralization (Figure 4G). However, neutralization of the electrical activity did not interfere with the neuroprotective effect of both ghrelin and Dln101 (Figure 4H). Altogether,

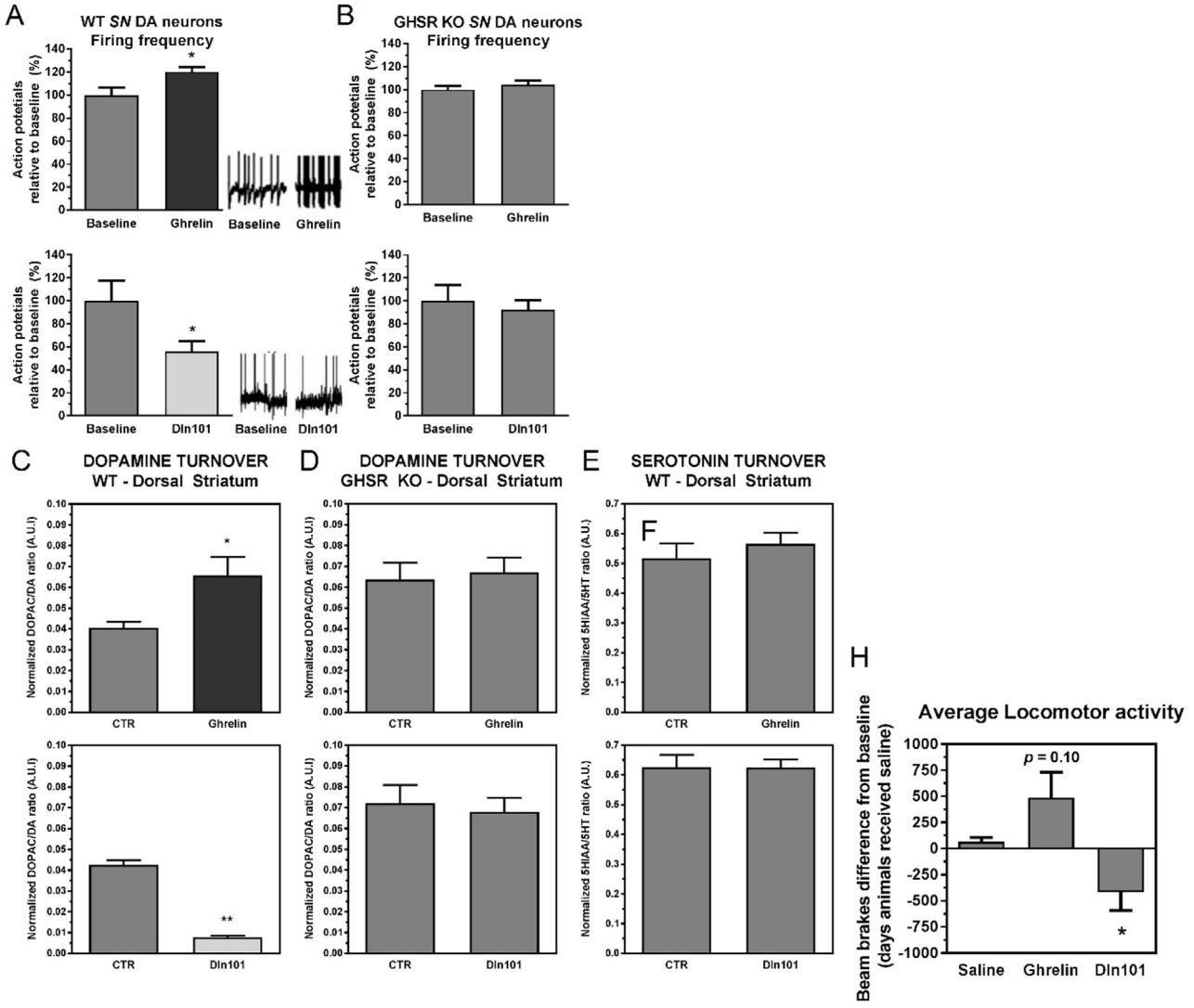

Figure 3: Effects of ghrelin and Dln101 over *SN* DA neuron function of GHSR KO mice and their WT littermates. (A) Using patch-clamp slice electrophysiology analysis, the firing frequency (generation of action potentials) was recorded in *SN* DA neurons for 15 min followed by acute ghrelin (1 μM) or Dln101 (1 μM) administration. In WT neurons, ghrelin increased (120.3% relative to baseline) neuronal activity whereas Dln101 decreased it (55.5%). **(B)** No effect was observed in GHSR KO animals. Paired t test; n = 4–13 per group. **(C)** Dopamine turnover (DOPAC/DA ratio) was evaluated by HPLC-ED 30 min after s.c. administration of saline (CTR), ghrelin 15 nM, or Dln101 15 nM. In WT mice, ghrelin promoted increased dorsal striatum dopamine release (CTR = 0.040 ± 0.002, Ghrelin = 0.066 ± 0.009, top graph). After Dln101 administration, dopamine release was reduced in dorsal striatum (CTR = 0.038 ± 0.002, Dln101 = 0.005 ± 0.001, bottom graph). Unpaired t tests, n = 4–5. **(D)** Dopamine release in dorsal striatum of GHSR KO animals was unaffected by ghrelin or Dln101. Unpaired t tests, n = 3–4. **(E)** For control purposes, serotonin turnover (5HIAA/5HT) was quantified in dorsal striatum following ghrelin or Dln101 injection and no change was observed. Unpaired t tests, n = 5–7. **(F)** Average locomotor activity was evaluated by infrared monitoring up to 3 h after subcutaneous administration of saline, ghrelin 15 nM, or Dln101 15 nM. Total number of beam breaks on the day of ghrelin/Dln101 administration was subtracted from total number of beam breaks from the day before, when animals received saline (baseline). Ghrelin promoted a tendency to increase average locomotor activity (p = 0.10) whereas Dln101-injected animals had the opposite effect, promoting a substantial decrease in locomotor activity. Paired t test; n = 4 per group. All other data were analyzed using unpaired t tests.

our data suggest that modulation of electrical activity of *SN* DA cells is completely irrelevant for acyl-ghrelin or Dln101-mediated neuroprotection in the MPTP-induced neurodegeneration model.

3.5. Dln101 and ghrelin have opposite effects over *SN* DA neuron mitochondria

Mitochondrial dynamics has a direct impact over mitochondrial functions and thus is of central importance for the pathophysiology of neurodegenerative processes. However, the *in vivo* significance of changes in mitochondrial dynamics in the context of nigrostriatal dopaminergic cells has remained undetermined. We decided to evaluate mitochondrial morphology following ghrelin and Dln101 treatment and its impact on neuroprotection of *SN* DA cells using electron microscopy. Initially, we compared animals treated with either Dln101 or ghrelin for 10 consecutive days under the same protocol used to achieve neuroprotection. Analysis of the distribution of mitochondrial area demonstrated a higher percentage of bigger mitochondria in *SN* DA cells from Dln101-treated animals, compared to controls, shifting the histogram curve to the right and indicative of increased fusion (Figure 5A,B). Average mitochondrial area was also increased following Dln101 treatment (Figure 5C). No change in area was observed in the ghrelin-treated group (Figure 5A–C).

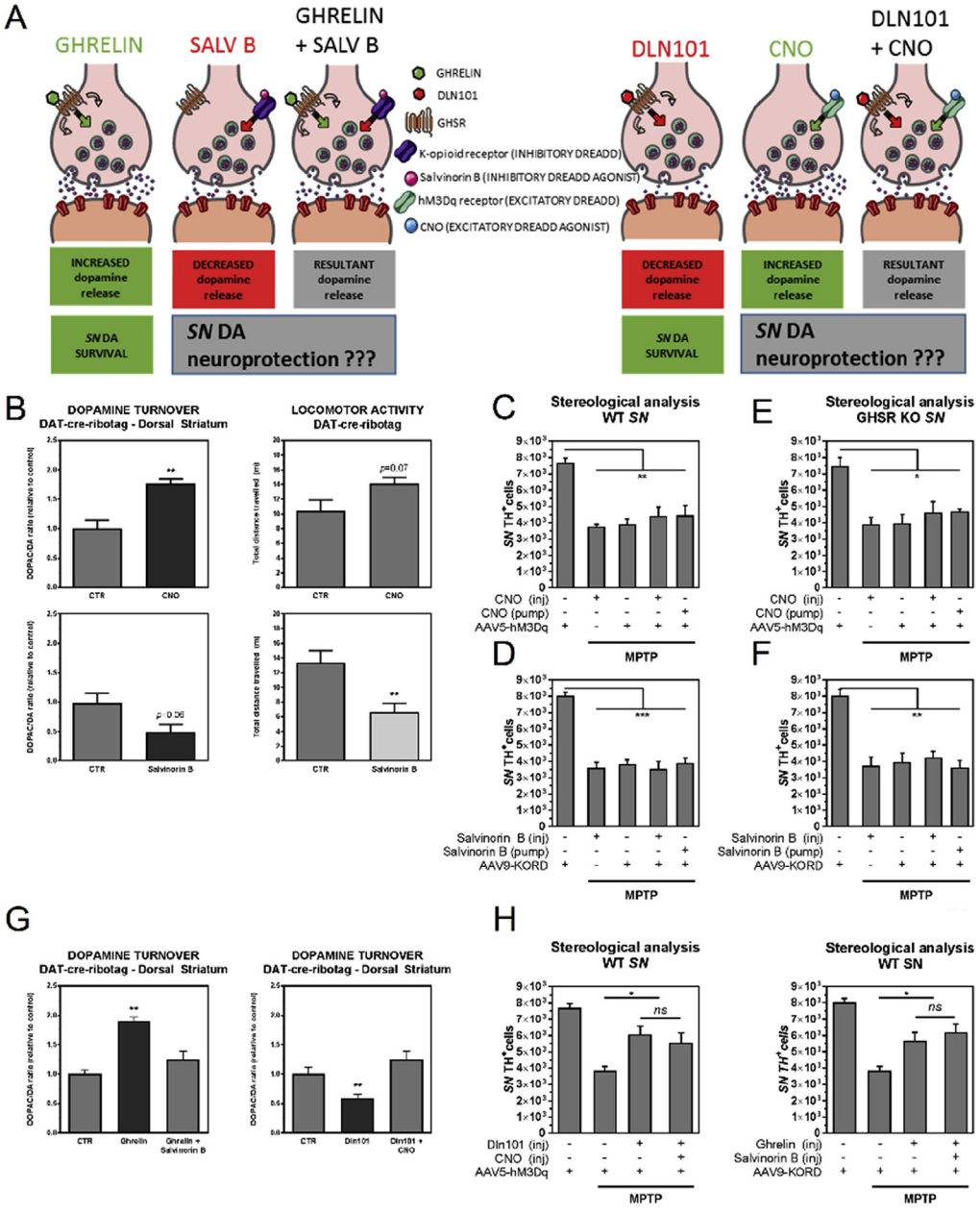

Figure 4: Modulation of electrical activity of *SN* DA neurons and its effects on survival, dopamine release in dorsal striatum, and locomotor activity in DAT-cre-ribotag mice. **(A)** GHSR-mediated protection of substantia nigra dopamine neurons by ghrelin or Dln101 occurs despite their opposite effects on neuronal electrical activity. To address whether modulation of electrical activity is sufficient or necessary for neuroprotection, we used DREADDs to evaluate neuroprotection in scenarios of controlled neuronal firing. **(B)** Dopamine turnover (DOPAC/DA ratio) and locomotor activity in DAT-cre-ribotag mice was evaluated 30–45 min after subcutaneous administration of vehicle (CTR), CNO (0.3 mg/kg) or Salvinorin B (5 mg/kg). Excitatory DREADD activation with CNO promoted elevated dopamine release in dorsal striatum in comparison to saline (CTR = 1.00 ± 0.13, CNO = 1.77 ± 0.08), n = 3. Inhibitory DREADD activation with Salvinorin B produced a tendency towards decreased dopamine release (CTR = 1.00 ± 0.47, Salvinorin B = 0.55 ± 0.16), n = 5. Animals had their locomotor activity recorded for 10 min. CNO promoted a tendency towards increased locomotor activity, while Salvinorin B decreased it (CTR = 10.87 ± 2.01, CNO = 13.62 ± 0.90) and (CTR = 13.37 ± 1.61, Salvinorin B = 6.67 ± 1.17). Unpaired t test; n = 3–10 per group. **(C)** Total number of TH^+ cells in *SN* was evaluated in WT animals with expression of excitatory DREADD. CNO (0.3 mg/kg) was injected daily using the same routine used for ghrelin and Dln101 administration, or chronically released using osmotic minipump placed in the interscapular space. MPTP administration promoted vast nigral degeneration that was not prevented by the excitatory DREADD agonist, in any of the delivery formats. **(D)** Total number of TH^+ cells in *SN* was evaluated in WT animals with expression of inhibitory DREADD. Salvinorin B (5 mg/kg) was injected or chronic released using osmotic minipump. **(E)** Total number of TH^+ cells in *SN* was evaluated in GHSR KO animals with expression of excitatory DREADD. **(F)** Total number of TH^+ cells in *SN* was evaluated in GHSR KO animals with expression of inhibitory DREADD. **(G)** Ghrelin-induced increase in dopamine release in dorsal striatum was prevented with injection of Salvinorin B in animals with expression of inhibitory DREADD. Likewise, Dln101-induced decrease in dopamine release in dorsal striatum was prevented with injection of CNO in animals with expression of excitatory DREADD. **(H)** Dln101 and ghrelin displayed their neuroprotective effect even with neutralization of their effects on neuronal firing. Data from C to H were analyzed using One-way ANOVA test followed by multiple comparisons test, n = 6–8 per group.

Mitochondrial cytoplasmic coverage was not changed in the Dln101 group but was increased in the ghrelin group, suggesting increased mitochondrial biogenesis promoted by ghrelin (Figure 5D), as previously described [12]. Next, we decided to evaluate changes in mitochondrial morphology following MPTP exposure (15 mg/kg) and how pre-treatment with Dln101 would impact mitochondrial changes. Animals were euthanized at 2 different time points: 4 h, and 1 day after MPTP exposure. At the 4-hours' time point, MPTP-treated animals displayed a shift to the left in the mitochondrial histogram curve and a decrease in average mitochondrial area, all indicative of increased fission (Figure 5E–G, red). No change in mitochondrial cytoplasmic coverage was observed (Figure 5H). Surprisingly, 1 day after MPTP exposure, we actually observed a shift to the right in the mitochondrial histogram curve and an increase in average mitochondrial area (Figure 5E–G, orange). However, a marked decrease in mitochondrial cytoplasmic coverage was observed (Figure 5H), indicative of degeneration of small mitochondria and preservation of bigger mitochondria, shifting the population towards bigger mitochondria but in lower number. Interestingly, animals pre-treated with Dln101 before MPTP displayed a more pronounced shifting to the right on the mitochondrial histogram curve at 1-day time point, with associated increase in the average area of remaining mitochondria (Figure 5E–G, green). Additionally, no changes in cytoplasmic coverage were observed. Taken together, our working hypothesis was that MPTP treatment initially leads to mitochondrial fragmentation, with following degeneration of small and preservation of bigger mitochondria. Dln101 treatment induces fusion of mitochondria and therefore protects mitochondria against MPTP-induced fragmentation and degeneration.

To support the idea of Dln101-induced mitochondrial fusion, we decided to evaluate the expression of several genes related to the control of mitochondrial dynamics. Using DAT-cre-ribotag animals, we compared the gene expression between controls, Dln101, ghrelin, and MPTP-treated (all after 4h) animals. For genes involved with mitochondrial fission (Fis-1, Mff and Drp-1), no change was observed with Dln101 treatment. Ghrelin treatment led to an increase in Mff and MPTP treatment increased expression of Drp-1, the main regulator of mitochondrial fission. For genes related to mitochondrial fusion (Mitofusin 1 and 2, Opa-1), Dln101 treatment led to an increase in mfn 2 expression, but not in mfn 1. No change in these two genes was observed with ghrelin treatment. Inversely, MPTP treatment led to a markedly decrease in both mitofusins expression. Taken together, real-time pcr data indeed support the notion of increased mitochondrial fission following MPTP treatment and increased mitochondrial fusion following Dln101 treatment (Figure 5I). Moreover, data suggests that mfn2 might have an important role in this process.

3.6. Knockout of mitochondrial fusion protein 2 (MFN 2) blocks DLN101-induced mitochondrial fusion in *SN* DA neurons

To determine if mfn2 is indeed a key factor controlling mitochondrial fusion and Dln101-mediated neuroprotection in *SN* DA cells, we generated mice with tamoxifen-induced deletion of mfn 2 gene in dopamine cells (iCre-DAT$^{MFN2\ KO}$). Mice were allowed normal development and had their series of tamoxifen injections between 4 and 6 weeks of age. Deletion of mfn2 gene *per se* in dopamine cells did not alter dorsal striatum dopamine levels, number of *SN* DA cells, locomotor activity (Figure 6A–C), or generated any noticeable behavioral alteration on these animals, checked until 4 months after tamoxifen exposure. Electron microscopy analysis of mitochondria of iCre-DAT$^{MFN2\ KO}$ *SN* DA cells revealed no changes in mitochondrial morphology, area, or coverage (Figure 6D,E). However, when iCre-DAT$^{MFN2\ KO}$ animals were treated with Dln101, no increased rate of fusion was observed (Figure 6F–H).

3.7. Knockout of MFN 2 prevents DLN101 neuroprotective effect and, in combination with MPTP, induces an aberrant mitochondria phenotype *SN* DA cells

Lack of increased fusion in the Dln101-treated iCre-DAT$^{MFN2\ KO}$ animals was correlated with absence of neuroprotection against MPTP, as evaluated by total TH^{+} cell number in *SN* of those animals (Figure 7A), and motor performance in the rotarod test (Figure 7B). In fact, MPTP-treated iCre-DAT$^{MFN2\ KO}$ animals displayed loss of small mitochondria, leading to an increase in average mitochondrial area, but to a decrease in both total number of mitochondria per cell and mitochondrial cytoplasmic coverage (Figure 7D). This was similar to what was observed in WT animals (Figure 5E), after 1 day of MPTP-exposure. Noteworthy, in MPTP-treated iCre-DAT$^{MFN2\ KO}$ animals, these changes in mitochondrial content happened already 4 h after MPTP challenge. Finally, swollen mitochondria, with unidentifiable cristae, typical of dysfunctional, mitophagy-prone mitochondria was predominant in iCre-DAT$^{MFN2\ KO}$ animals after 3 days of MPTP challenge (Figure 7C), leading to a further increase in both average mitochondrial area and coverage (Figure 7D). Supporting the notion of severe loss of mitochondrial content, we observed a continuous drop in the average number of mitochondrial units per cell following MPTP exposure (Figure 7D).

4. DISCUSSION

Ghrelin is mainly produced in the X/A-like gland cells of the gastric fundus mucosa [44] and, to a lesser degree, in the intestines, pancreas, gall bladder, liver, gonads, and breasts [45]. Ghrelin peptide is formed after post-translational processing of the 117-amino-acid peptide preproghrelin. Then, native ghrelin peptide is subject to a unique modification consisting of acylation (addition of an octanoyl group) of the third serine residue (Ser3), a process well conserved among mammalian species [46]. The enzyme responsible for ghrelin acylation, before its secretion, is known as ghrelin-O-acyl-transferase (GOAT), and is predominantly expressed in gastrointestinal organs [47,48]. According to its acylation status, the peptide can be termed des-acyl or acyl ghrelin. De-acylation process is performed by esterases, including acyl-protein thioesterase-1/lysophospholipase-1 (APT-1), thought to be mainly responsible for ghrelin de-acylation *in vivo* [49].

Physiological action of acyl ghrelin gene products specifically in the midbrain has been matter of debate as ghrelin does not seem to be expressed in the central nervous system [50,51] despite immunolabeling in arcuate nucleus neurons [52,53], and some cells around the third ventricle [54]. On one hand, although only acyl ghrelin is able to activate GHSR, 66–94% of circulating ghrelin is actually found in the des-acyl form [55–57], due to the activity of esterases and APT-1 [49]. In addition, ghrelin has a limited capacity to cross the blood-brain-barrier [58]. On the other hand, Dln101 emerges as a relevant candidate to maintain GHSR activation due to its increased stability in the acylated residue.

Des-acyl ghrelin is the predominant form of ghrelin, but the lack of acylation precludes it from binding to GHSR and subsequent receptor activation. Despite this, there are several reports describing des-acyl ghrelin's biological effects, including neuroprotection [59] and attenuation of proinflammatory cytokines release [60]. Despite the biological importance of des-acyl ghrelin has started to be elucidated, chronic administration of des-acyl ghrelin was shown inefficient in mitigating MPTP-induced *SN* DA neuronal degeneration in ghrelin KO animals

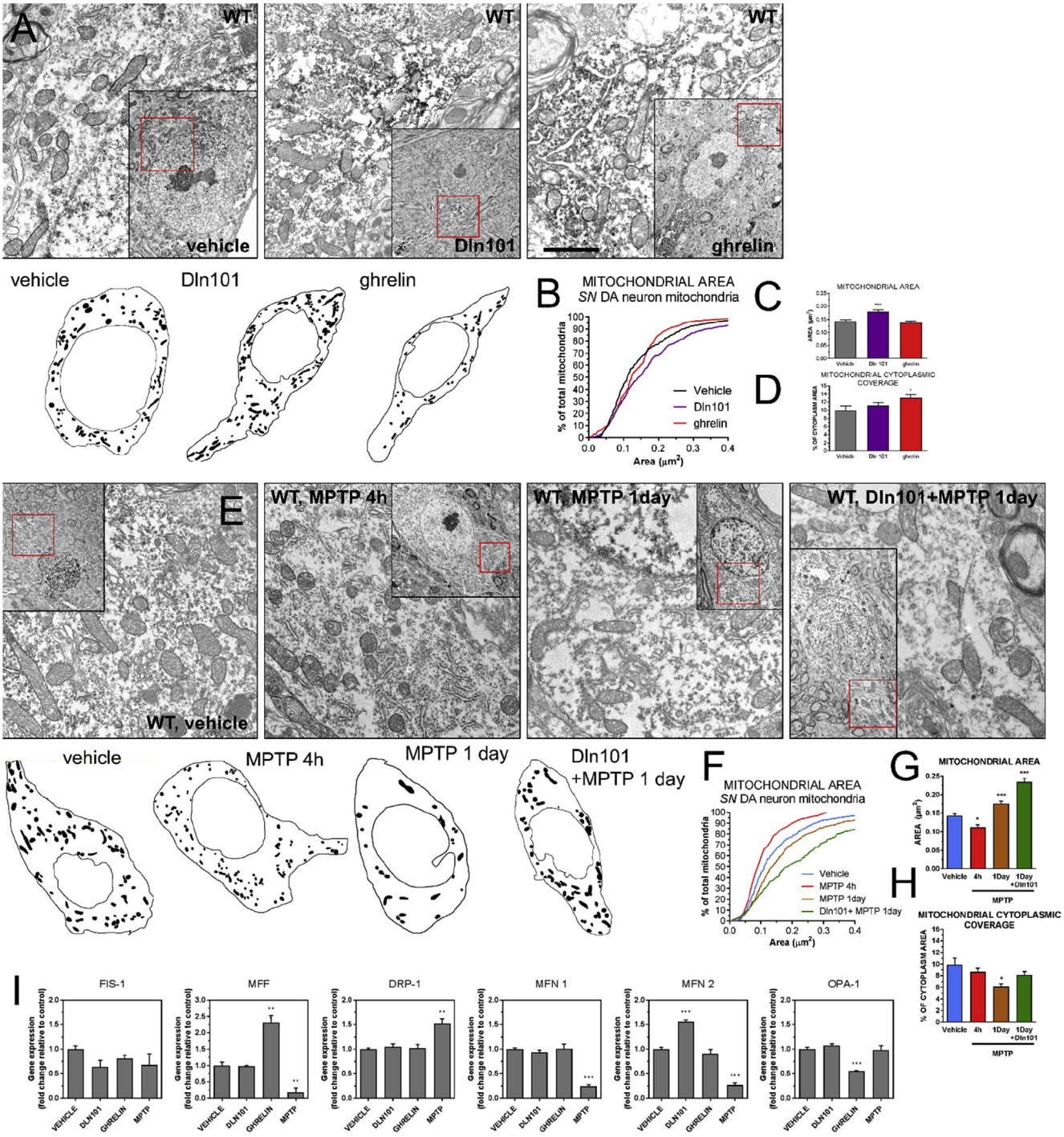

Figure 5: Effect of ghrelin and Dln101 on mitochondrial dynamics of WT *SN* DA neurons. **(A)** Representative EM pictures of WT *SN* DA cells under various treatments, with drawing of overall mitochondrial distribution in the representative cell. Scale bar = 1 μm **(B)** Cumulative probability distribution for mitochondrial area (vehicle = black, Dln101 = purple, ghrelin = red). Kolmogorov–Smirnov test, n = 315–555 per group. **(C)** Mitochondrial average area (vehicle = 0.143 ± 0.004, Dln101 = 0.181 ± .006, ghrelin = 0.138 ± .004, in μm^2). **(D)** Mitochondrial cytoplasmic coverage (vehicle = 9.94% ± 1.1, Dln101 = 11.2% ± 0.75, ghrelin = 13.05% ± 0.79, as percentage of total cytoplasm area). Area and coverage were analyzed using One-way ANOVA followed by multiple comparisons test; n = 315–555 per group. **(E)** MPTP-induced mitochondrial fragmentation and degeneration in *SN* DA neurons. Representative EM pictures of *SN* DA cells. **(F)** Cumulative probability distribution for mitochondrial area (vehicle = blue, MPTP 4h = red, MPTP 1day = orange, Dln101 + MPTP 1day = green). **(G)** Mitochondrial average area (vehicle = 0.143 ± 0.004, MPTP 4h = 0.112 ± 0.006, MPTP 1day = 0.176 ± 0.006, Dln101 + MPTP 1day = 0.234 ± 0.009). **(H)** Mitochondrial cytoplasmic coverage (vehicle = 9.94% ± 1.1, MPTP 4h = 8.66% ± 0.68, MPTP 1day = 6.144% ± 0.51, Dln101 + MPTP 1day = 8.14% ± 0.55). Kolmogorov–Smirnov test on cumulative distribution, One-way ANOVA on G and H; n = 102–473 per group. **(I)** Real-time PCR data of genes coding mitochondrial fission (FIS-1, MFF, DRP-1) and fusion proteins (MFN 1, MFN 2, OPA-1) at 4h time point. One-way ANOVA test followed by multiple comparisons test; n = 4–7 per group.

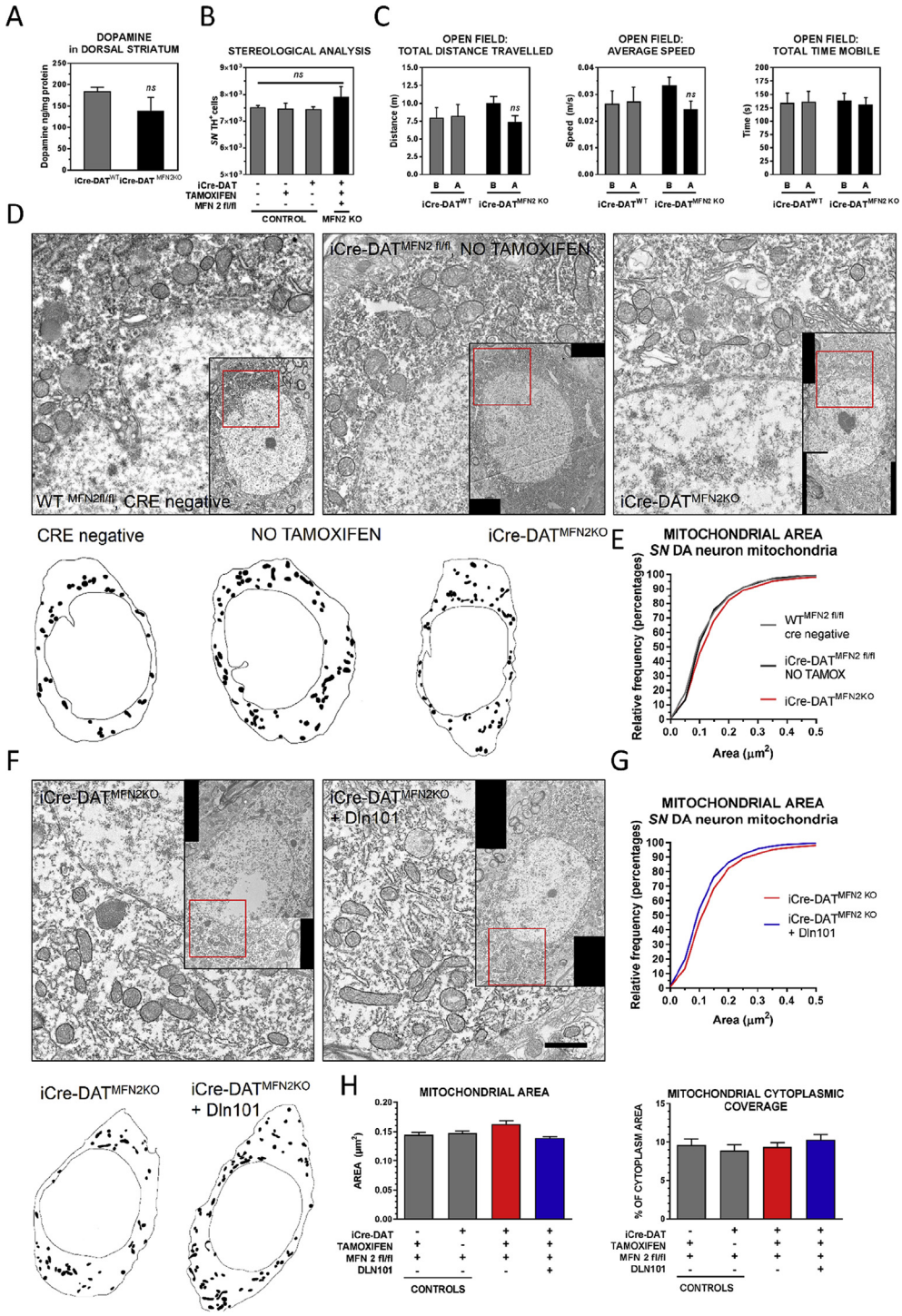

Figure 6: Mitofusin 2 deletion in DA neurons. **(A)** HPLC measurement of dorsal striatum dopamine levels (iCre-DAT^{WT} = 184.9 ± 9.1, iCre-DAT^{MFN2KO} = 139.4 ± 30.5, in ng/mg of tissue protein) Unpaired *t*-test, n = 4–5. **(B)** *SN* DA neuron number did not differ between control groups and iCre-DAT^{MFN2KO} animals (Controls = 7532 ± 62, 7482 ± 198, 7464 ± 86; iCre-DAT^{MFN2KO} = 7912 ± 383), One-way ANOVA, *n* = 3–7. **(C)** Open field locomotor behavior analysis (B = before, A = after tamoxifen injections; iCre-DAT^{WT} grey bars and iCre-DAT^{MFN2KO} black bars; Total distance travelled (iCre-DAT^{WT}, B = 8.0 ± 1.7, A = 8.2 ± 1.9; iCre-DAT^{MFN2KO}, B = 10.0 ± 1.0, A = 7.4 ± 0.91; in meters). Average speed (iCre-DAT^{WT}, B = 0.026 ± 0.005, A = 0.027 ± 0.005; iCre-DAT^{MFN2KO}, B = 0.033 ± .003, A = 0.025 ± 0.003; in meters/second). Total time mobile (iCre-DAT^{WT}, B = 134 ± 19, A = 136 ± 20; iCre-DAT^{MFN2KO}, B = 138 ± 14, A = 132 ± 13, in seconds), total behavior test time was 300 s. Two-way ANOVA analysis retrieved no statistically significant differences, n = 11–14. **(D)** Representative EM pictures of *SN* DA cells of control (WT, either cre negative or iCre-DAT$^{MFN2\ fl/fl}$ animals that did not receive tamoxifen) and iCre-DAT^{MFN2KO} animals, with drawing of overall mitochondrial distribution in the representative cell. **(E)** Cumulative probability distribution for mitochondrial area (cre negative = grey, no tamoxifen = black, iCre-DAT^{MFN2KO} = red). No change was observed between groups. Kolmogorov–Smirnov test, n = 421–723 per group. **(F)** Dln101 does not induce mitochondrial fusion in iCre-DAT^{MFN2KO} animals. Representative EM pictures of *SN* DA cells. **(G)** Differently of what was observed in WT animals, Dln101 treatment did not induce a shift to the right in the cumulative distribution curve, suggesting no increased rate of mitochondrial fusion observed in iCre-DAT^{MFN2KO} animals. **(H)** No change in mitochondrial average area, or mitochondrial cytoplasmic coverage was observed with Dln101 treatment in iCre-DAT^{MFN2KO} animals. One-way ANOVA test followed by multiple comparisons test, n = 421–723 per group.

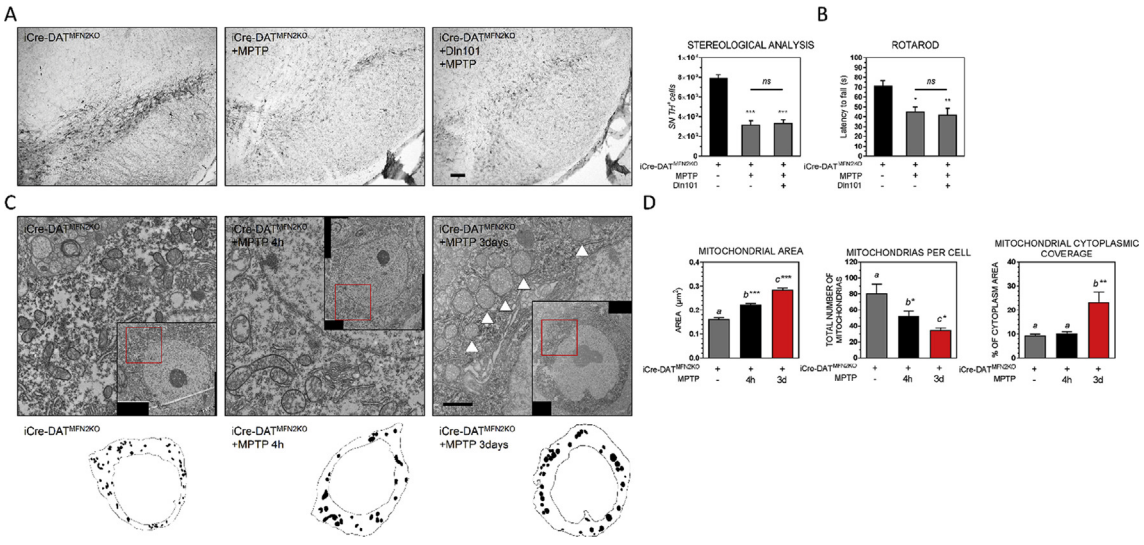

Figure 7: Mitofusin 2 deletion in DA neurons prevents Dln101 neuroprotective effect. **(A)** Visualization of TH^+ cells in DAB immunohistological preparation. Scale bar 100 μm. Stereological analysis indicates Dln101 administration did not mitigate MPTP-induced degeneration of *SN* DA cells in iCre-DAT^{MFN2KO} animals (iCre-DAT^{MFN2KO} = 7912 ± 383, iCre-DAT^{MFN2KO} + MPTP = 3205 ± 390, iCre-DAT^{MFN2KO} + Dln101 + MPTP = 3375 ± 329). One-way ANOVA test followed by multiple comparisons test, n = 4–6. **(B)** Dln101 treatment in iCre-DAT^{MFN2KO} animals did not prevent MPTP-induced decreased motor performance, assessed in the rotarod test (latency to fall, iCre-DAT^{MFN2KO} = 71.5 ± 5.1, iCre-DAT^{MFN2KO} + MPTP = 45.3 ± 4.7, iCre-DAT^{MFN2KO} + Dln101 + MPTP = 42.0 ± 6.9; in seconds). One-way ANOVA test followed by multiple comparisons test, n = 5–10. **(C)** Representative EM pictures of *SN* DA cells of iCre-DAT^{MFN2KO} animals after MPTP exposure. MPTP administration induced aberrant mitochondria phenotype, with surviving neurons displaying bigger and rounder mitochondria, indicated with arrowheads. Remaining mitochondria showed circular cristae, and abnormal inner membrane structures. **(D)** Aberrant mitochondria phenotype reflected in much higher average mitochondrial area (iCre-DAT^{MFN2KO} = 0.163 ± 0.005, iCre-DAT^{MFN2KO} + MPTP 4h = 0.179 ± 0.004, iCre-DAT^{MFN2KO} + MPTP 3days = 0.287 ± 0.006), but fewer mitochondrial units per cell (iCre-DAT^{MFN2KO} = 80 ± 12, iCre-DAT^{MFN2KO} + MPTP 4h = 52 ± 6, iCre-DAT^{MFN2KO} + MPTP 3days = 29 ± 3). Finally, mitochondrial coverage was drastically increased after 3 days of MPTP exposure, indicating the fewer but enormous remaining mitochondria doubled the covered cytoplasmic area when compared to the other groups (iCre-DAT^{MFN2KO} = 9.35% ± 0.56, iCre-DAT^{MFN2KO} + MPTP 4h = 10.22 ± 0.69, iCre-DAT^{MFN2KO} + MPTP 3days = 23.32 ± 4.21). One-way ANOVA test followed by multiple comparisons test, n = 421–1456.

[61], suggesting that the neuroprotective effect of ghrelin over *SN* DA cells indeed requires GHSR activation. Another possible explanation for midbrain action of ghrelin gene products is based on the local activity of GOAT [62], which mRNA has been shown to have a broad expression among tissues [63], including the central nervous system [64,65]. This fact supports the idea that ghrelin gene products could potentially be acylated *in situ,* permitting local activation of GHSR [66]. The potential therapeutic actions of GHSR in the central nervous system has been in the limelight lately. Peripheral administration of GHSR agonists have been shown to inhibit oxidative stress, apoptosis, proinflammatory cytokine production, microglia activation, mitochondrial dysfunction, and excitotoxicity both *in vivo* and *in vitro* [16,67–71], as well as exert neuroprotective effects against hippocampal and cortical neuronal death [68,72–74]. Through these actions, GHSR has thus been linked to neuroprotection in several CNS diseases such as stroke [75], Alzheimer disease [72,76], Parkinson disease [11–13,69,77], multiple sclerosis [78,79], epilepsy [80,81], and spinal cord injury [82]. Nevertheless, GHSRs have been shown to display higher constitutive basal activity in the absence of ligand [83], suggesting that (1) GHSR-mediated pathways do not need acyl ghrelin gene products to be activated but are modulated by them; (2) the existence of other(s) endogenous ligand(s) able to regulate GHSR activity in the midbrain and other brain areas.

In different cell types and tissues, acyl-ghrelin binds GHSR to activate several intracellular cascades, including ERK 1/2, PI3K/Akt/mTOR, and AMPK signaling pathways, thus mediating different physiological functions. The first described pathway associated with GHSR activation was the inositol 1,4,5-trisphosphate/diacylglycerol (IP3/DAG) pathway, leading to GH release in the anterior pituitary. In other non-neuronal tissues and cell types, the binding of acyl-ghrelin to GHSR activates either the phospholipase C/inositol trisphosphate or the adenylate cyclase/protein kinase A pathways, resulting in an increase in intracellular calcium levels. These activation of these different signaling pathways could be due to different endogenous ligands, differential concentration of acyl ghrelin [84], and/or differential GHSR dimerization to other receptors (as described for dopamine, serotonin, melanocortin receptors, among others) [85–88]. In *SN* DA cells, mitochondrial function is regulated to some extent by 5′-AMP-activated protein kinase (AMPK), a ubiquitous enzyme that is considered a master sensor of intracellular energy stress that plays a crucial role in adaptive responses to falling energy levels (e.g., from low nutrient availability or cellular stress). AMPK signaling is activated by GHSR and declines in PD patients [89]. Ghrelin-mediated activation of AMPK is associated with neuroprotection of *SN* DA cells [13,14]. Thus, activating AMPK may be an effective neuroprotective strategy to help restore energy balance and redox homeostasis in *SN* DA neurons, but other signaling pathways might also be involved in GHSR-mediated neuroprotection and must be considered. GHSR-mediated activation of AMPK is also observed in other brain regions, including the arcuate nucleus of the hypothalamus [90]. Further characterization of GHSR-mediated signaling pathways is required to support the development of clinical therapeutics targeting GHSR in *SN* DA cells to promote survival.

Oxidative stress, reactive gliosis, and T-cell infiltration are major pathological features in human PD and are recapitulated in the mouse MPTP model [91]. Oxidative stress defines an imbalance between the levels of reactive oxygen species (ROS) and reactive nitrogen species

(RNS) produced and the ability of a biological system to detoxify those reactive intermediates. Generation of ROS and RNS involves the activity of mitochondria and are impacted by mitochondrial dynamics. In *SN* DA neurons, oxidative stress can not only compromise protein function but also generate lipid peroxidation [92] and DNA fragmentation, ultimately leading to cell death. In addition, impairment of dopamine synthesis has been observed as a result of oxidation of tyrosine hydroxylase (TH) in the MPTP model [93].

In PD, the roles of oxidative stress and reactive gliosis are supported by postmortem brain tissue analyses (reviewed in [91]). Overall, activated glial cells contribute to increase local oxidative stress [94] and increase proinflammatory cytokine production [91]. Reactive gliosis happens as a consequence of cellular stress and can be divided in two major features: microglia activation and reactivation of astroglia. Specifically in the MPTP model, microglial activation precedes the loss of DA neurons and upregulation of proinflammatory cytokines [95]. Interventions that halt microglial activation have a direct impact on *SN* DA neuroprotection [96]. Reactive astrogliosis and T-cell infiltration in the *SN* are also present in the MPTP model [97,98], and neuroprotection of *SN* DA cell is achieved with strategies that tackle either one of those features [99–101]. Here, we demonstrated that DIn101 treatment was correlated with decreases in TH^+ cell oxidative stress, and microglia activation, as measured by decreased CD68 expression in *SN* region, similar to observed in interventions in monkeys [102]. We also reported prevention of upregulation of proinflammatory genes such as TNFα and the inflammasome component Nrlp3, both of which have been associated with MPTP-induced loss of *SN* DA neurons [103,104]. Moreover, DIn101 ability to activate GHSR might have a deeper relevance to neuroprotection beyond regulation of mitochondrial dynamics, once GHSR signaling has been linked to negative control of neuroinflammation [104,105], which is believed to sustain and exacerbate the loss of the DA neurons in PD. Taken together, our data suggest that DIn101 can act in different components of the pathophysiology of *SN* DA neurodegeneration, perhaps providing a better outcome in clinical therapies for PD.

Another key component of proper DA cell physiology is the basal firing activity of *SN* DA neurons, which maintains extracellular levels of dopamine in the dorsal striatum that are essential for voluntary movement [106]. Changes in *SN* DA neuron activity directly impacts the amount of dopamine released in target areas and are largely observed in PD subjects [107] as well as in PD animal models and may occur in the absence of changes in other indirect markers of DA neuron function (e.g. neuron number, DA content) [108,109].

The proper control of *SN* DA cell electrical activity is of crucial importance because, on one hand and despite the yet elusive mechanism underlying such effect and identification of all cell types involved [110], augmentation of electrical activity of *SN* DA neurons is thought to be neuroprotective, as increased survival of DA cells has been reported with the use of depolarizing agents such as veratridine [19] and K^+ [111]. Also in line with these observations, prospective cohort and case–control studies have identified tobacco smoking as the most significant protective factor against the risk of developing PD, decreasing it by 60% in active cigarette smokers in comparison to those who never smoked [112,113]. The mechanisms involved includes reinforcing cholinergic stimulation of *SN* DA neurons with nicotine, which also showed to be protective in mouse and monkey MPTP models [114–116]. Consistently, degeneration of DA neurons has been observed in situations of diminished electrical activity [117,118], including the use of MPTP, which is linked to the activation of KATP channels and consequently silencing of *SN* DA neurons [119]. Interestingly, KATP channels-mediated hyperpolarization of *SN* DA neurons induced by mitochondrial dysfunction was mediated by mitochondrial reactive oxygen species (ROS) [120]. These data suggest that ROS could possibly participate in the demise of *SN* DA neurons by rendering them electrically inactive [121].

One another hand, *SN* DA neuron activity and dopamine release relies on a controlled modulation of cytosolic calcium levels [122]. Overactivation of *SN* DA cells leads to excitotoxicity, causing mitochondrial dysfunction and ultimately neuronal degeneration. Therefore, the fine balance between excitation/inhibition is mandatory for proper *SN* DA cell function. Based on that, we decided to investigate effects of electrical activity *per se* on *SN* DA neuroprotection but also on GHSR-mediated neuroprotection. Our data suggest that, at least for the acute mouse MPTP model, modulation of electrical activity is not associated with neuroprotection and, in fact, is not required for GHSR-mediated ghrelin and DIn101 neuroprotection.

Mitochondrial dynamics are tightly coordinated in association with the cell cycle and state, with complex structural and functional interactions leading to fusion and fission of mitochondria to alter the balance of oxidative phosphorylation, rescue damaged mitochondria and regulate reactive oxygen species production. Mitochondrial dynamics are also central to the pathogenesis of idiopathic and toxin-induced cases of PD, as well as several monogenic familial PD forms. Mitochondrial length is the result of competitive balance between GTPase dynamin-like proteins mediators of mitochondrial fusion and fission. Mitofusin 1 (MFN1) and 2 (MFN2), located in the outer mitochondrial membrane, and optic atrophy protein 1 (OPA1), in the inner membrane, regulate mitochondrial fusion whereas dynamin-related protein 1 (DRP1) regulates mitochondrial fission; among other supporting proteins involved [27,28]. Disruption of mitochondrial fission leads to an extensively interconnected and collapsed mitochondrial network, while defects in mitochondrial fusion lead to mitochondrial fragmentation and loss of mitochondrial DNA. As a promoter of mitochondrial fusion, DIn101 is thought to facilitate the exchange of mitochondrial DNA, protein components, and metabolites required for mitochondrial function, conferring increased resilience against MPTP-induced cellular stress. Efficient mitochondrial fusion is important for cell viability, because cells defective in fusion exhibit reduced growth, decreased mitochondrial membrane potential ($\Delta\Psi_m$), and defective respiration, resulting in impaired cellular energy metabolism [123,124], exactly as observed in patients with PD [125], in both sporadic and genetic forms of the disease [126].

In fact, changes in mitochondrial dynamics directly affects many things including cellular metabolism [127], mitochondrial mass and turnover [128], mitochondrial transport, and calcium buffering [129]. Nigrostriatal DA neurons seem to have a preferential susceptibility to loss of Mfn2 when compared to VTA DA neurons [130]. Although a specific mitochondrial fusion or fission protein has not been implicated in classic PD, recent data suggest that impaired mitochondrial fusion due to mutations in Opa1 cause parkinsonism in the absence of clinically significant optic atrophy [131]. Furthermore, it is well known that α-synuclein and MPTP cause fragmentation of mitochondria [132]. Taken together, these studies support the notion that interventions to increase mitochondrial fusion are crucial to re-establish proper *SN* DA neuronal function and avoid neurodegeneration, as demonstrated in [133,134]. Moreover, Rappold and colleagues [134] suggest that increased mitochondrial fusion not only can be a strategy to prevent neurodegeneration but also can be used to restore proper function of remaining cells, as impairment in mitochondrial dynamics also disrupts synaptic release of dopamine. Spared TH^+ cells in PD patients and animal models of PD after establishment of Parkisonism could benefit from mitochondrial fusion inducing agents to re-establish proper synaptic dopamine release and thus ameliorate the symptoms of PD.

Finally, disruption of cellular metabolism is a key feature of PD, with both α-synuclein and PD-related neurotoxins such as MPTP acting as disruptors [135,136]. Bioenergetic failure produced by these and other factors may also contribute to the degeneration of vulnerable neurons, such as SN DA cells. Dopamine neurons of the *SN* are particularly vulnerable to energy failure because of their substantial energy demands. Neurons in general consume a huge amount of energy in order to maintain the ionic gradient across their plasma membrane. SN DA neurons have long unmyelinated axons and extensive arborization making their energy demands especially high [137,138]. Furthermore, they exhibit pacemaking activity that maintains basal DA tone across an expansive region, increasing their energy demands even further [139]. Neurons do not store glycogen so they are especially sensitive to fluctuations in energy demand and reliant on neighboring astrocytes to provide nutrients [140]. Unfortunately, *SN* DA neurons have relatively few surrounding astrocytes to provide supplementary energy [140]. Thus, the nigrostriatal DA system is probably the most vulnerable neuronal population to compromised bioenergetic status [141], becoming very sensitive to changes in mitochondrial dynamics that impact oxidative capacity and cellular bioenergetics.

AUTHOR CONTRIBUTION

BS, MN, ZWL, XBG, LM, and TLH designed the experiments. BS, CN, MN, DC, ZWL, XBG, JDE, and LM performed experiments. BS, LM, and TLH designed the project and wrote the paper.

ACKNOWLEDGEMENTS

This study was supported by NIH grants AG052005, AG052986, AG051459, DK111178 and NKFI-126998 from the Hungarian National Research, Development and Innovation Office (T.L.H), and the Michael J. Fox Foundation.
B.S. and M.N. are recipients of the Science without Borders fellowships from The Brazilian Federal Agency for Support and Assessment of Post-graduate Education (CAPES) and from the National Council for Scientific and Technological Development (CNPq), respectively.

CONFLICT OF INTEREST

The authors declare no conflict of interest regarding studies of this paper.

REFERENCES

[1] Shaikh, S.I., Verma, H., 2011. Parkinson's disease and anaesthesia. Indian Journal of Anaesthesia 55(3):228–234.
[2] Dorsey, E.R., Constantinescu, R., Thompson, J.P., Biglan, K.M., Holloway, R.G., Kieburtz, K., et al., 2007. Projected number of people with Parkinson disease in the most populous nations, 2005 through 2030. Neurology 68(5):384–386.
[3] Bernheimer, H., Birkmayer, W., Hornykiewicz, O., Jellinger, K., Seitelberger, F., 1973. Brain dopamine and the syndromes of Parkinson and Huntington. Clinical, morphological and neurochemical correlations. Journal of the Neurological Sciences 20(4):415–455.
[4] Carlsson, A., 1993. Thirty years of dopamine research. Advances in Neurology 60:1–10.
[5] Hornykiewicz, O., 1993. Parkinson's disease and the adaptive capacity of the nigrostriatal dopamine system: possible neurochemical mechanisms. Advances in Neurology 60:140–147.
[6] Fahn, S., 2015. The medical treatment of Parkinson disease from James Parkinson to George Cotzias. Movement Disorders 30(1):4–18.
[7] Morton, G.J., Meek, T.H., Schwartz, M.W., 2014. Neurobiology of food intake in health and disease. Nature Reviews Neuroscience 15(6):367–378.
[8] Malik, S., McGlone, F., Bedrossian, D., Dagher, A., 2008. Ghrelin modulates brain activity in areas that control appetitive behavior. Cell Metabolism 7(5):400–409.
[9] Horvath, T.L., Diano, S., Tschop, M., 2003. Ghrelin in hypothalamic regulation of energy balance. Current Topics in Medicinal Chemistry 3(8):921–927.
[10] Zigman, J.M., Jones, J.E., Lee, C.E., Saper, C.B., Elmquist, J.K., 2006. Expression of ghrelin receptor mRNA in the rat and the mouse brain. Journal of Comparative Neurology 494(3):528–548.
[11] Jiang, H., Li, L.J., Wang, J., Xie, J.X., 2008. Ghrelin antagonizes MPTP-induced neurotoxicity to the dopaminergic neurons in mouse substantia nigra. Experimental Neurology 212(2):532–537.
[12] Andrews, Z.B., Erion, D., Beiler, R., Liu, Z.W., Abizaid, A., Zigman, J., et al., 2009. Ghrelin promotes and protects nigrostriatal dopamine function via a UCP2-dependent mitochondrial mechanism. Journal of Neuroscience 29(45):14057–14065.
[13] Bayliss, J.A., Andrews, Z.B., 2013. Ghrelin is neuroprotective in Parkinson's disease: molecular mechanisms of metabolic neuroprotection. Therapeutic Advances in Endocrinology and Metabolism 4(1):25–36.
[14] Bayliss, J.A., Lemus, M.B., Stark, R., Santos, V.V., Thompson, A., Rees, D.J., et al., 2016. Ghrelin-AMPK signaling mediates the neuroprotective effects of calorie restriction in Parkinson's disease. Journal of Neuroscience 36(10):3049–3063.
[15] Baatar, D., Patel, K., Taub, D.D., 2011. The effects of ghrelin on inflammation and the immune system. Molecular and Cellular Endocrinology 340(1):44–58.
[16] Zhou, C.H., Li, X., Zhu, Y.Z., Huang, H., Li, J., Liu, L., et al., 2014. Ghrelin alleviates neuropathic pain through GHSR-1a-mediated suppression of the p38 MAPK/NF-kappaB pathway in a rat chronic constriction injury model. Regional Anesthesia and Pain Medicine 39(2):137–148.
[17] Dragicevic, E., Schiemann, J., Liss, B., 2015. Dopamine midbrain neurons in health and Parkinson's disease: emerging roles of voltage-gated calcium channels and ATP-sensitive potassium channels. Neuroscience 284:798–814.
[18] Michel, P.P., Toulorge, D., Guerreiro, S., Hirsch, E.C., 2013. Specific needs of dopamine neurons for stimulation in order to survive: implication for Parkinson disease. The FASEB Journal 27(9):3414–3423.
[19] Salthun-Lassalle, B., Hirsch, E.C., Wolfart, J., Ruberg, M., Michel, P.P., 2004. Rescue of mesencephalic dopaminergic neurons in culture by low-level stimulation of voltage-gated sodium channels. Journal of Neuroscience 24(26):5922–5930.
[20] Gonon, F.G., Buda, M.J., 1985. Regulation of dopamine release by impulse flow and by autoreceptors as studied by in vivo voltammetry in the rat striatum. Neuroscience 14(3):765–774.
[21] Michel, P.P., Alvarez-Fischer, D., Guerreiro, S., Hild, A., Hartmann, A., Hirsch, E.C., 2007. Role of activity-dependent mechanisms in the control of dopaminergic neuron survival. Journal of Neurochemistry 101(2):289–297.
[22] Mihaylova, M.M., Shaw, R.J., 2011. The AMPK signalling pathway coordinates cell growth, autophagy and metabolism. Nature Cell Biology 13(9):1016–1023.
[23] Rambold, A.S., Kostelecky, B., Elia, N., Lippincott-Schwartz, J., 2011. Tubular network formation protects mitochondria from autophagosomal degradation during nutrient starvation. Proceedings of the National Academy of Sciences of the United States of America 108(25):10190–10195.
[24] Gomes, L.C., Di Benedetto, G., Scorrano, L., 2011. During autophagy mitochondria elongate, are spared from degradation and sustain cell viability. Nature Cell Biology 13(5):589–598.

[25] Chan, D.C., 2006. Dissecting mitochondrial fusion. Developmental Cell 11(5): 592–594.
[26] Youle, R.J., Karbowski, M., 2005. Mitochondrial fission in apoptosis. Nature Reviews Molecular Cell Biology 6(8):657–663.
[27] Itoh, K., Nakamura, K., Iijima, M., Sesaki, H., 2013. Mitochondrial dynamics in neurodegeneration. Trends in Cell Biology 23(2):64–71.
[28] Archer, S.L., 2013. Mitochondrial dynamics–mitochondrial fission and fusion in human diseases. New England Journal of Medicine 369(23):2236–2251.
[29] Knott, A.B., Perkins, G., Schwarzenbacher, R., Bossy-Wetzel, E., 2008. Mitochondrial fragmentation in neurodegeneration. Nature Reviews Neuroscience 9(7):505–518.
[30] Zhu, J., Chu, C.T., 2010. Mitochondrial dysfunction in Parkinson's disease. Journal of Alzheimers Disease 20(Suppl 2):S325–S334.
[31] Toulorge, D., Schapira, A.H., Hajj, R., 2016. Molecular changes in the postmortem parkinsonian brain. Journal of Neurochemistry 139(Suppl 1): 27–58.
[32] Zhao, F., Wang, W., Wang, C., Siedlak, S.L., Fujioka, H., Tang, B., et al., 2017. Mfn2 protects dopaminergic neurons exposed to paraquat both in vitro and in vivo: implications for idiopathic Parkinson's disease. Biochimica et Biophysica Acta 1863(6):1359–1370.
[33] Gasser, T., 2007. Update on the genetics of Parkinson's disease. Movement Disorders 22(Suppl 17):S343–S350.
[34] Lee, Y., Dawson, V.L., Dawson, T.M., 2012. Animal models of Parkinson's disease: vertebrate genetics. Cold Spring Harbor Perspectives in Medicine 2(10).
[35] Bender, A., Krishnan, K.J., Morris, C.M., Taylor, G.A., Reeve, A.K., Perry, R.H., et al., 2006. High levels of mitochondrial DNA deletions in substantia nigra neurons in aging and Parkinson disease. Nature Genetics 38(5):515–517.
[36] Kraytsberg, Y., Kudryavtseva, E., McKee, A.C., Geula, C., Kowall, N.W., Khrapko, K., 2006. Mitochondrial DNA deletions are abundant and cause functional impairment in aged human substantia nigra neurons. Nature Genetics 38(5):518–520.
[37] Ballard, P.A., Tetrud, J.W., Langston, J.W., 1985. Permanent human parkinsonism due to 1-methyl-4-phenyl-1,2,3,6-tetrahydropyridine (MPTP): seven cases. Neurology 35(7):949–956.
[38] Langston, J.W., 2017. The MPTP story. Journal of Parkinson's Disease 7(s1): S11–S19.
[39] Schapira, A.H., Cooper, J.M., Dexter, D., Clark, J.B., Jenner, P., Marsden, C.D., 1990. Mitochondrial complex I deficiency in Parkinson's disease. Journal of Neurochemistry 54(3):823–827.
[40] Dietrich, M.O., Liu, Z.W., Horvath, T.L., 2013. Mitochondrial dynamics controlled by mitofusins regulate Agrp neuronal activity and diet-induced obesity. Cell 155(1):188–199.
[41] Abizaid, A., Liu, Z.W., Andrews, Z.B., Shanabrough, M., Borok, E., Elsworth, J.D., et al., 2006. Ghrelin modulates the activity and synaptic input organization of midbrain dopamine neurons while promoting appetite. Journal of Clinical Investigation 116(12):3229–3239.
[42] Paxinos, G., Franklin, K., 2001. The mouse brain in stereotaxic coordinates, 3 ed. Academic Press. p. 256.
[43] Stutz, B., da Conceicao, F.S., Santos, L.E., Cadilhe, D.V., Fleming, R.L., Acquarone, M., et al., 2014. Murine dopaminergic Muller cells restore motor function in a model of Parkinson's disease. Journal of Neurochemistry 128(6):829–840.
[44] Kojima, M., Hosoda, H., Date, Y., Nakazato, M., Matsuo, H., Kangawa, K., 1999. Ghrelin is a growth-hormone-releasing acylated peptide from stomach. Nature 402(6762):656–660.
[45] Gnanapavan, S., Kola, B., Bustin, S.A., Morris, D.G., McGee, P., Fairclough, P., et al., 2002. The tissue distribution of the mRNA of ghrelin and subtypes of its receptor, GHS-R, in humans. The Journal of Clinical Endocrinology & Metabolism 87(6):2988.
[46] Nishi, Y., Yoh, J., Hiejima, H., Kojima, M., 2011. Structures and molecular forms of the ghrelin-family peptides. Peptides 32(11):2175–2182.
[47] Gutierrez, J.A., Solenberg, P.J., Perkins, D.R., Willency, J.A., Knierman, M.D., Jin, Z., et al., 2008. Ghrelin octanoylation mediated by an orphan lipid transferase. Proceedings of the National Academy of Sciences of the United States of America 105(17):6320–6325.
[48] Yang, J., Brown, M.S., Liang, G., Grishin, N.V., Goldstein, J.L., 2008. Identification of the acyltransferase that octanoylates ghrelin, an appetite-stimulating peptide hormone. Cell 132(3):387–396.
[49] Satou, M., Nishi, Y., Yoh, J., Hattori, Y., Sugimoto, H., 2010. Identification and characterization of acyl-protein thioesterase 1/lysophospholipase I as a ghrelin deacylation/lysophospholipid hydrolyzing enzyme in fetal bovine serum and conditioned medium. Endocrinology 151(10):4765–4775.
[50] Furness, J.B., Hunne, B., Matsuda, N., Yin, L., Russo, D., Kato, I., et al., 2011. Investigation of the presence of ghrelin in the central nervous system of the rat and mouse. Neuroscience 193:1–9.
[51] Francois, M., Barde, S., Achamrah, N., Breton, J., do Rego, J.C., Coeffier, M., et al., 2015. The number of preproghrelin mRNA expressing cells is increased in mice with activity-based anorexia. Neuropeptides 51:17–23.
[52] Lu, S., Guan, J.L., Wang, Q.P., Uehara, K., Yamada, S., Goto, N., et al., 2002. Immunocytochemical observation of ghrelin-containing neurons in the rat arcuate nucleus. Neuroscience Letters 321(3):157–160.
[53] Kageyama, H., Kitamura, Y., Hosono, T., Kintaka, Y., Seki, M., Takenoya, F., et al., 2008. Visualization of ghrelin-producing neurons in the hypothalamic arcuate nucleus using ghrelin-EGFP transgenic mice. Regulatory Peptides 145(1–3):116–121.
[54] Cowley, M.A., Smith, R.G., Diano, S., Tschop, M., Pronchuk, N., Grove, K.L., et al., 2003. The distribution and mechanism of action of ghrelin in the CNS demonstrates a novel hypothalamic circuit regulating energy homeostasis. Neuron 37(4):649–661.
[55] Yoshimoto, A., Mori, K., Sugawara, A., Mukoyama, M., Yahata, K., Suganami, T., et al., 2002. Plasma ghrelin and desacyl ghrelin concentrations in renal failure. Journal of the American Society of Nephrology 13(11):2748–2752.
[56] Patterson, M., Murphy, K.G., le Roux, C.W., Ghatei, M.A., Bloom, S.R., 2005. Characterization of ghrelin-like immunoreactivity in human plasma. The Journal of Clinical Endocrinology & Metabolism 90(4):2205–2211.
[57] Tong, J., Dave, N., Mugundu, G.M., Davis, H.W., Gaylinn, B.D., Thorner, M.O., et al., 2013. The pharmacokinetics of acyl, des-acyl, and total ghrelin in healthy human subjects. European Journal of Endocrinology 168(6):821–828.
[58] Rhea, E.M., Salameh, T.S., Gray, S., Niu, J., Banks, W.A., Tong, J., 2018. Ghrelin transport across the blood-brain barrier can occur independently of the growth hormone secretagogue receptor. Molecular Metabolism 18:88–96.
[59] Chung, H., Seo, S., Moon, M., Park, S., 2008. Phosphatidylinositol-3-kinase/Akt/glycogen synthase kinase-3 beta and ERK1/2 pathways mediate protective effects of acylated and unacylated ghrelin against oxygen-glucose deprivation-induced apoptosis in primary rat cortical neuronal cells. Journal of Endocrinology 198(3):511–521.
[60] Bulgarelli, I., Tamiazzo, L., Bresciani, E., Rapetti, D., Caporali, S., Lattuada, D., et al., 2009. Desacyl-ghrelin and synthetic GH-secretagogues modulate the production of inflammatory cytokines in mouse microglia cells stimulated by beta-amyloid fibrils. Journal of Neuroscience Research 87(12):2718–2727.
[61] Bayliss, J.A., Lemus, M., Santos, V.V., Deo, M., Elsworth, J., Andrews, Z.B., 2016. Acylated but not des-acyl ghrelin is neuroprotective in an MPTP mouse model of Parkinson's Disease. Journal of Neurochemistry 137(3):460–471.
[62] Hopkins, A.L., Nelson, T.A., Guschina, I.A., Parsons, L.C., Lewis, C.L., Brown, R.C., et al., 2017. Unacylated ghrelin promotes adipogenesis in rodent bone marrow via ghrelin O-acyl transferase and GHS-R1a activity: evidence for target cell-induced acylation. Scientific Reports 7:45541.

[63] Lim, C.T., Kola, B., Grossman, A., Korbonits, M., 2011. The expression of ghrelin O-acyltransferase (GOAT) in human tissues. Endocrine Journal 58(8): 707–710.

[64] Gahete, M.D., Cordoba-Chacon, J., Kineman, R.D., Luque, R.M., Castano, J.P., 2011. Role of ghrelin system in neuroprotection and cognitive functions: implications in Alzheimer's disease. Peptides 32(11):2225–2228.

[65] Gahete, M.D., Cordoba-Chacon, J., Salvatori, R., Castano, J.P., Kineman, R.D., Luque, R.M., 2010. Metabolic regulation of ghrelin O-acyl transferase (GOAT) expression in the mouse hypothalamus, pituitary, and stomach. Molecular and Cellular Endocrinology 317(1–2):154–160.

[66] Murtuza, M.I., Isokawa, M., 2018. Endogenous ghrelin-O-acyltransferase (GOAT) acylates local ghrelin in the hippocampus. Journal of Neurochemistry 144(1):58–67.

[67] Lee, J.Y., Yune, T.Y., 2014. Ghrelin inhibits oligodendrocyte cell death by attenuating microglial activation. Endocrinology and Metabolism (Seoul) 29(3):371–378.

[68] Zhang, R., Yang, G., Wang, Q., Guo, F., Wang, H., 2013. Acylated ghrelin protects hippocampal neurons in pilocarpine-induced seizures of immature rats by inhibiting cell apoptosis. Molecular Biology Reports 40(1):51–58.

[69] Beynon, A.L., Brown, M.R., Wright, R., Rees, M.I., Sheldon, I.M., Davies, J.S., 2013. Ghrelin inhibits LPS-induced release of IL-6 from mouse dopaminergic neurones. Journal of Neuroinflammation 10:40.

[70] Yang, M., Hu, S., Wu, B., Miao, Y., Pan, H., Zhu, S., 2007. Ghrelin inhibits apoptosis signal-regulating kinase 1 activity via upregulating heat-shock protein 70. Biochemical and Biophysical Research Communications 359(2): 373–378.

[71] Chung, H., Kim, E., Lee, D.H., Seo, S., Ju, S., Lee, D., et al., 2007. Ghrelin inhibits apoptosis in hypothalamic neuronal cells during oxygen-glucose deprivation. Endocrinology 148(1):148–159.

[72] Moon, M., Choi, J.G., Nam, D.W., Hong, H.S., Choi, Y.J., Oh, M.S., et al., 2011. Ghrelin ameliorates cognitive dysfunction and neurodegeneration in intrahippocampal amyloid-beta1-42 oligomer-injected mice. Journal of Alzheimers Disease 23(1):147–159.

[73] Miao, Y., Xia, Q., Hou, Z., Zheng, Y., Pan, H., Zhu, S., 2007. Ghrelin protects cortical neuron against focal ischemia/reperfusion in rats. Biochemical and Biophysical Research Communications 359(3):795–800.

[74] Lee, J., Lim, E., Kim, Y., Li, E., Park, S., 2010. Ghrelin attenuates kainic acid-induced neuronal cell death in the mouse hippocampus. Journal of Endocrinology 205(3):263–270.

[75] Kenny, R., Cai, G., Bayliss, J.A., Clarke, M., Choo, Y.L., Miller, A.A., et al., 2013. Endogenous ghrelin's role in hippocampal neuroprotection after global cerebral ischemia: does endogenous ghrelin protect against global stroke? American Journal of Physiology Regulatory Integrative and Comparative Physiology 304(11):R980–R990.

[76] Moon, M., Cha, M.Y., Mook-Jung, I., 2014. Impaired hippocampal neurogenesis and its enhancement with ghrelin in 5XFAD mice. Journal of Alzheimers Disease 41(1):233–241.

[77] Moon, M., Kim, H.G., Hwang, L., Seo, J.H., Kim, S., Hwang, S., et al., 2009. Neuroprotective effect of ghrelin in the 1-methyl-4-phenyl-1,2,3,6-tetrahydropyridine mouse model of Parkinson's disease by blocking microglial activation. Neurotoxicity Research 15(4):332–347.

[78] Theil, M.M., Miyake, S., Mizuno, M., Tomi, C., Croxford, J.L., Hosoda, H., et al., 2009. Suppression of experimental autoimmune encephalomyelitis by ghrelin. The Journal of Immunology 183(4):2859–2866.

[79] Souza-Moreira, L., Delgado-Maroto, V., Morell, M., O'Valle, F., Del Moral, R.G., Gonzalez-Rey, E., 2013. Therapeutic effect of ghrelin in experimental autoimmune encephalomyelitis by inhibiting antigen-specific Th1/Th17 responses and inducing regulatory T cells. Brain Behavior and Immunity 30:54–60.

[80] Lucchi, C., Curia, G., Vinet, J., Gualtieri, F., Bresciani, E., Locatelli, V., et al., 2013. Protective but not anticonvulsant effects of ghrelin and JMV-1843 in the pilocarpine model of Status epilepticus. PLoS One 8(8):e72716.

[81] Portelli, J., Michotte, Y., Smolders, I., 2012. Ghrelin: an emerging new anticonvulsant neuropeptide. Epilepsia 53(4):585–595.

[82] Lee, J.Y., Choi, H.Y., Na, W.H., Ju, B.G., Yune, T.Y., 2014. Ghrelin inhibits BSCB disruption/hemorrhage by attenuating MMP-9 and SUR1/TrpM4 expression and activation after spinal cord injury. Biochimica et Biophysica Acta 1842(12 Pt A):2403–2412.

[83] Holst, B., Cygankiewicz, A., Jensen, T.H., Ankersen, M., Schwartz, T.W., 2003. High constitutive signaling of the ghrelin receptor–identification of a potent inverse agonist. Molecular Endocrinology 17(11):2201–2210.

[84] Stengel, A., Wang, L., Tache, Y., 2011. Stress-related alterations of acyl and desacyl ghrelin circulating levels: mechanisms and functional implications. Peptides 32(11):2208–2217.

[85] Kern, A., Albarran-Zeckler, R., Walsh, H.E., Smith, R.G., 2012. Apo-ghrelin receptor forms heteromers with DRD2 in hypothalamic neurons and is essential for anorexigenic effects of DRD2 agonism. Neuron 73(2): 317–332.

[86] Schellekens, H., van Oeffelen, W.E., Dinan, T.G., Cryan, J.F., 2013. Promiscuous dimerization of the growth hormone secretagogue receptor (GHS-R1a) attenuates ghrelin-mediated signaling. Journal of Biological Chemistry 288(1):181–191.

[87] Girardet, C., Mavrikaki, M., Southern, M.R., Smith, R.G., Butler, A.A., 2014. Assessing interactions between Ghsr and Mc3r reveals a role for AgRP in the expression of food anticipatory activity in male mice. Endocrinology 155(12): 4843–4855.

[88] Kern, A., Mavrikaki, M., Ullrich, C., Albarran-Zeckler, R., Brantley, A.F., Smith, R.G., 2015. Hippocampal dopamine/DRD1 signaling dependent on the ghrelin receptor. Cell 163(5):1176–1190.

[89] Curry, D.W., Stutz, B., Andrews, Z.B., Elsworth, J.D., 2018. Targeting AMPK signaling as a neuroprotective strategy in Parkinson's disease. Journal of Parkinson's Disease 8(2):161–181.

[90] Theander-Carrillo, C., Wiedmer, P., Cettour-Rose, P., Nogueiras, R., Perez-Tilve, D., Pfluger, P., et al., 2006. Ghrelin action in the brain controls adipocyte metabolism. Journal of Clinical Investigation 116(7):1983–1993.

[91] Cebrian, C., Loike, J.D., Sulzer, D., 2015. Neuroinflammation in Parkinson's disease animal models: a cell stress response or a step in neurodegeneration? Current Topics in Behavioral Neurosciences 22:237–270.

[92] Perier, C., Tieu, K., Guegan, C., Caspersen, C., Jackson-Lewis, V., Carelli, V., et al., 2005. Complex I deficiency primes Bax-dependent neuronal apoptosis through mitochondrial oxidative damage. Proceedings of the National Academy of Sciences of the United States of America 102(52):19126–19131.

[93] Ara, J., Przedborski, S., Naini, A.B., Jackson-Lewis, V., Trifiletti, R.R., Horwitz, J., et al., 1998. Inactivation of tyrosine hydroxylase by nitration following exposure to peroxynitrite and 1-methyl-4-phenyl-1,2,3,6-tetrahydropyridine (MPTP). Proceedings of the National Academy of Sciences of the United States of America 95(13):7659–7663.

[94] Mander, P., Borutaite, V., Moncada, S., Brown, G.C., 2005. Nitric oxide from inflammatory-activated glia synergizes with hypoxia to induce neuronal death. Journal of Neuroscience Research 79(1–2):208–215.

[95] Czlonkowska, A., Kohutnicka, M., Kurkowska-Jastrzebska, I., Czlonkowski, A., 1996. Microglial reaction in MPTP (1-methyl-4-phenyl-1,2,3,6-tetrahydropyridine) induced Parkinson's disease mice model. Neurodegeneration 5(2):137–143.

[96] Subramaniam, S.R., Federoff, H.J., 2017. Targeting microglial activation states as a therapeutic Avenue in Parkinson's disease. Frontiers in Aging Neuroscience 9:176.

[97] Yasuda, Y., Shimoda, T., Uno, K., Tateishi, N., Furuya, S., Yagi, K., et al., 2008. The effects of MPTP on the activation of microglia/astrocytes and

cytokine/chemokine levels in different mice strains. Journal of Neuroimmunology 204(1–2):43–51.

[98] Hirsch, E.C., Hunot, S., 2009. Neuroinflammation in Parkinson's disease: a target for neuroprotection? The Lancet Neurology 8(4):382–397.

[99] Brochard, V., Combadiere, B., Prigent, A., Laouar, Y., Perrin, A., Beray-Berthat, V., et al., 2009. Infiltration of CD4+ lymphocytes into the brain contributes to neurodegeneration in a mouse model of Parkinson disease. Journal of Clinical Investigation 119(1):182–192.

[100] Reynolds, A.D., Stone, D.K., Hutter, J.A., Benner, E.J., Mosley, R.L., Gendelman, H.E., 2010. Regulatory T cells attenuate Th17 cell-mediated nigrostriatal dopaminergic neurodegeneration in a model of Parkinson's disease. The Journal of Immunology 184(5):2261–2271.

[101] Manocha, G.D., Floden, A.M., Puig, K.L., Nagamoto-Combs, K., Scherzer, C.R., Combs, C.K., 2017. Defining the contribution of neuroinflammation to Parkinson's disease in humanized immune system mice. Molecular Neurodegeneration 12(1):17.

[102] Swanson, C.R., Joers, V., Bondarenko, V., Brunner, K., Simmons, H.A., Ziegler, T.E., et al., 2011. The PPAR-gamma agonist pioglitazone modulates inflammation and induces neuroprotection in parkinsonian monkeys. Journal of Neuroinflammation 8:91.

[103] Sriram, K., Matheson, J.M., Benkovic, S.A., Miller, D.B., Luster, M.I., O'Callaghan, J.P., 2002. Mice deficient in TNF receptors are protected against dopaminergic neurotoxicity: implications for Parkinson's disease. The FASEB Journal 16(11):1474–1476.

[104] Yan, Y., Jiang, W., Liu, L., Wang, X., Ding, C., Tian, Z., et al., 2015. Dopamine controls systemic inflammation through inhibition of NLRP3 inflammasome. Cell 160(1–2):62–73.

[105] Shao, W., Zhang, S.Z., Tang, M., Zhang, X.H., Zhou, Z., Yin, Y.Q., et al., 2013. Suppression of neuroinflammation by astrocytic dopamine D2 receptors via alphaB-crystallin. Nature 494(7435):90–94.

[106] Tepper, J.M., Creese, I., Schwartz, D.H., 1991. Stimulus-evoked changes in neostriatal dopamine levels in awake and anesthetized rats as measured by microdialysis. Brain Research 559(2):283–292.

[107] Karachi, C., Grabli, D., Bernard, F.A., Tande, D., Wattiez, N., Belaid, H., et al., 2010. Cholinergic mesencephalic neurons are involved in gait and postural disorders in Parkinson disease. Journal of Clinical Investigation 120(8):2745–2754.

[108] Branch, S.Y., Chen, C., Sharma, R., Lechleiter, J.D., Li, S., Beckstead, M.J., 2016. Dopaminergic neurons exhibit an age-dependent decline in electrophysiological parameters in the MitoPark mouse model of Parkinson's disease. Journal of Neuroscience 36(14):4026–4037.

[109] Rice, M.E., Patel, J.C., Cragg, S.J., 2011. Dopamine release in the basal ganglia. Neuroscience 198:112–137.

[110] Mourlevat, S., Troadec, J.D., Ruberg, M., Michel, P.P., 2003. Prevention of dopaminergic neuronal death by cyclic AMP in mixed neuronal/glial mesencephalic cultures requires the repression of presumptive astrocytes. Molecular Pharmacology 64(3):578–586.

[111] Douhou, A., Troadec, J.D., Ruberg, M., Raisman-Vozari, R., Michel, P.P., 2001. Survival promotion of mesencephalic dopaminergic neurons by depolarizing concentrations of K+ requires concurrent inactivation of NMDA or AMPA/kainate receptors. Journal of Neurochemistry 78(1):163–174.

[112] van der Mark, M., Nijssen, P.C., Vlaanderen, J., Huss, A., Mulleners, W.M., Sas, A.M., et al., 2014. A case-control study of the protective effect of alcohol, coffee, and cigarette consumption on Parkinson disease risk: time-since-cessation modifies the effect of tobacco smoking. PLoS One 9(4):e95297.

[113] de Lau, L.M., Breteler, M.M., 2006. Epidemiology of Parkinson's disease. The Lancet Neurology 5(6):525–535.

[114] Parain, K., Hapdey, C., Rousselet, E., Marchand, V., Dumery, B., Hirsch, E.C., 2003. Cigarette smoke and nicotine protect dopaminergic neurons against the 1-methyl-4-phenyl-1,2,3,6-tetrahydropyridine Parkinsonian toxin. Brain Research 984(1–2):224–232.

[115] Parain, K., Marchand, V., Dumery, B., Hirsch, E., 2001. Nicotine, but not cotinine, partially protects dopaminergic neurons against MPTP-induced degeneration in mice. Brain Research 890(2):347–350.

[116] Quik, M., Chen, L., Parameswaran, N., Xie, X., Langston, J.W., McCallum, S.E., 2006. Chronic oral nicotine normalizes dopaminergic function and synaptic plasticity in 1-methyl-4-phenyl-1,2,3,6-tetrahydropyridine-lesioned primates. Journal of Neuroscience 26(17):4681–4689.

[117] Patil, N., Cox, D.R., Bhat, D., Faham, M., Myers, R.M., Peterson, A.S., 1995. A potassium channel mutation in weaver mice implicates membrane excitability in granule cell differentiation. Nature Genetics 11(2):126–129.

[118] Katsuki, H., Takenaka, C., Kume, T., Kaneko, S., Akaike, A., 2001. Requirement of neural activity for the maintenance of dopaminergic neurons in rat midbrain slice cultures. Neuroscience Letters 300(3):166–170.

[119] Liss, B., Haeckel, O., Wildmann, J., Miki, T., Seino, S., Roeper, J., 2005. K-ATP channels promote the differential degeneration of dopaminergic midbrain neurons. Nature Neuroscience 8(12):1742–1751.

[120] Bao, L., Avshalumov, M.V., Rice, M.E., 2005. Partial mitochondrial inhibition causes striatal dopamine release suppression and medium spiny neuron depolarization via H2O2 elevation, not ATP depletion. Journal of Neuroscience 25(43):10029–10040.

[121] Avshalumov, M.V., Chen, B.T., Koos, T., Tepper, J.M., Rice, M.E., 2005. Endogenous hydrogen peroxide regulates the excitability of midbrain dopamine neurons via ATP-sensitive potassium channels. Journal of Neuroscience 25(17):4222–4231.

[122] Chan, C.S., Guzman, J.N., Ilijic, E., Mercer, J.N., Rick, C., Tkatch, T., et al., 2007. 'Rejuvenation' protects neurons in mouse models of Parkinson's disease. Nature 447(7148):1081–1086.

[123] Franco, A., Kitsis, R.N., Fleischer, J.A., Gavathiotis, E., Kornfeld, O.S., Gong, G., et al., 2016. Correcting mitochondrial fusion by manipulating mitofusin conformations. Nature 540(7631):74–79.

[124] Bose, A., Beal, M.F., 2016. Mitochondrial dysfunction in Parkinson's disease. Journal of Neurochemistry 139(Suppl 1):216–231.

[125] Henchcliffe, C., Beal, M.F., 2008. Mitochondrial biology and oxidative stress in Parkinson disease pathogenesis. Nature Clinical Practice Neurology 4(11):600–609.

[126] Franco-Iborra, S., Vila, M., Perier, C., 2016. The Parkinson disease mitochondrial hypothesis: where are we at? The Neuroscientist 22(3):266–277.

[127] Detmer, S.A., Chan, D.C., 2007. Functions and dysfunctions of mitochondrial dynamics. Nature Reviews Molecular Cell Biology 8(11):870–879.

[128] Berthet, A., Margolis, E.B., Zhang, J., Hsieh, I., Zhang, J., Hnasko, T.S., et al., 2014. Loss of mitochondrial fission depletes axonal mitochondria in midbrain dopamine neurons. Journal of Neuroscience 34(43):14304–14317.

[129] Haddad, D., Nakamura, K., 2015. Understanding the susceptibility of dopamine neurons to mitochondrial stressors in Parkinson's disease. FEBS Letters 589(24 Pt A):3702–3713.

[130] Pham, A.H., Meng, S., Chu, Q.N., Chan, D.C., 2012. Loss of Mfn2 results in progressive, retrograde degeneration of dopaminergic neurons in the nigrostriatal circuit. Human Molecular Genetics 21(22):4817–4826.

[131] Carelli, V., Musumeci, O., Caporali, L., Zanna, C., La Morgia, C., Del Dotto, V., et al., 2015. Syndromic parkinsonism and dementia associated with OPA1 missense mutations. Annals of Neurology 78(1):21–38.

[132] Kamp, F., Exner, N., Lutz, A.K., Wender, N., Hegermann, J., Brunner, B., et al., 2010. Inhibition of mitochondrial fusion by alpha-synuclein is rescued by PINK1, Parkin and DJ-1. The EMBO Journal 29(20):3571–3589.

[133] Cui, M., Tang, X., Christian, W.V., Yoon, Y., Tieu, K., 2010. Perturbations in mitochondrial dynamics induced by human mutant PINK1 can be rescued by the mitochondrial division inhibitor mdivi-1. Journal of Biological Chemistry 285(15):11740–11752.

[134] Rappold, P.M., Cui, M., Grima, J.C., Fan, R.Z., de Mesy-Bentley, K.L., Chen, L., et al., 2014. Drp1 inhibition attenuates neurotoxicity and dopamine release deficits in vivo. Nature Communications 5:5244.

[135] Devi, L., Raghavendran, V., Prabhu, B.M., Avadhani, N.G., Anandatheerthavarada, H.K., 2008. Mitochondrial import and accumulation of alpha-synuclein impair complex I in human dopaminergic neuronal cultures and Parkinson disease brain. Journal of Biological Chemistry 283(14):9089–9100.

[136] Anandhan, A., Jacome, M.S., Lei, S., Hernandez-Franco, P., Pappa, A., Panayiotidis, M.I., et al., 2017. Metabolic dysfunction in Parkinson's disease: bioenergetics, redox homeostasis and central carbon metabolism. Brain Research Bulletin 133:12–30.

[137] Pacelli, C., Giguere, N., Bourque, M.J., Levesque, M., Slack, R.S., Trudeau, L.E., 2015. Elevated mitochondrial bioenergetics and axonal arborization size are key contributors to the vulnerability of dopamine neurons. Current Biology 25(18):2349–2360.

[138] Michel, P.P., Hirsch, E.C., Hunot, S., 2016. Understanding dopaminergic cell death pathways in Parkinson disease. Neuron 90(4):675–691.

[139] Guzman, J.N., Sanchez-Padilla, J., Wokosin, D., Kondapalli, J., Ilijic, E., Schumacker, P.T., et al., 2010. Oxidant stress evoked by pacemaking in dopaminergic neurons is attenuated by DJ-1. Nature 468(7324):696–700.

[140] Mena, M.A., Garcia de Yebenes, J., 2008. Glial cells as players in parkinsonism: the "good," the "bad," and the "mysterious" glia. The Neuroscientist 14(6):544–560.

[141] Pissadaki, E.K., Bolam, J.P., 2013. The energy cost of action potential propagation in dopamine neurons: clues to susceptibility in Parkinson's disease. Frontiers in Computational Neuroscience 7(13).

